Title:

Essential Function of Membrane-Bound Transcription Factor MYRF in Promoting Transcription of miRNA *lin-4* during *C. elegans* Development

Zhimin Xu[1], Zhao Wang[1], Lifang Wang[1,2], Yingchuan B. Qi[1,2,3]

Affiliations and Notes:

1. School of Life Science and Technology, ShanghaiTech University, Shanghai, 201210, China.

2. Correspondence: lifangwang06@gmail.com, qiyc@shanghaitech.edu.cn.

3. Lead contact: qiyc@shanghaitech.edu.cn

Abstract

Precise developmental timing control is essential for organism formation and function, but its mechanisms are unclear. In *C. elegans*, the microRNA *lin-4* plays a critical role in developmental timing. While *lin-4*'s downregulation of LIN-14 is well-established, the mechanisms behind *lin-4* upregulation remain unknown. We demonstrate that the membrane-associated transcription factor MYRF-1 is necessary for *lin-4* upregulation in late L1 stage. MYRF-1 is initially localized on the cell membrane, and its increased cleavage and nuclear accumulation coincide with *lin-4* expression timing. We show that MYRF-1 regulates *lin-4* expression cell-autonomously and that hyperactive MYRF-1 can prematurely drive *lin-4* expression in early L1 and embryos. The tandem *lin-4* promoter DNA recruits MYRF-1^{GFP} to form visible loci in the nucleus, suggesting that MYRF-1 directly acts on the *lin-4* promoter. Our findings identify a crucial link in understanding developmental timing regulation and establish MYRF-1 as a key regulator of *lin-4* expression.

Introduction

It is during the embryonic stage that the basic form and pattern of organisms are mostly established. However, the majority of growth in animals occurs during post-embryonic stages[1]. Some extreme examples are seen in insects undergoing metamorphosis and vertebrate amphibians[2]. In many cases, there is often a considerable increase in body size, but profound transitions take place, such as neural circuitry remodeling throughout juvenile years and sexual maturation[3-6]. Undoubtedly, the genetic program determines how different species grow to different characteristic sizes and forms, yet such mechanisms remain largely unknown. One key question is how developmental timing is controlled.

When hatching out of their egg shells, the nematode *C. elegans* exhibits a miniature yet grossly similar form to adults, and demonstrates a set of behavioral abilities including sensory response, locomotion, and learning[7-9]. They go through four larval stages before becoming fertile adults, and the transition between two consecutive larval stages is marked by a molting event. Changes in the temporal pattern of development are best exemplified by stage-specific cell division and differentiation of blast cells, as well as stage-specific epidermal cuticle formation fate. Such stage-specific patterns can be skipped or reiterated in so-called heterochronic mutants, and *lin-4* and *lin-14* are the two that have been studied in details[10-16]. *lin-4* mutants exhibit complex cell lineage defects, including reiterated larval stage 1-specific cell division in some progenitors, while *lin-14* mutants exhibit precocious patterning where stage-specific events are skipped. The studies of these mutants led to the discovery of the first microRNA regulatory pathway as follows: The ubiquitously expressed nuclear factor LIN-14 promotes L1 patterns and suppresses progression to L2. The microRNA *lin-4* is upregulated during late L1, and suppresses LIN-14 post-transcriptionally, consequently initiating progression to L2 pattern[17, 18]. *lin-4* - LIN-14 pair not only controls the division pattern of blast cells but also controls the maturation and plasticity of the neural circuit during L1-L2 transition[19-21]; *lin-4* is also involved in other diverse biological

processes[22]. The vertebrate ortholog of *lin-4*, known as *miR-125*, has been found to promote neuronal differentiation and maturation[23, 24].

What remains a mystery is the factors that trigger the expression of the *lin-4* microRNA during mid-late L1. It is known that the coding sequence of *lin-4* is embedded within an intron of a host gene, and its transcription uses its own promoter and bound Pol II complexes[13, 17, 25]. Once produced, *lin-4* can self-enhance its own transcription by directly interacting with cis-elements in the promoter region[26, 27]. It is also known that during embryonic stages, the transcription of *lin-4* is suppressed by FLYWCH transcriptional factors, but this suppression only extends until late embryogenesis[28]. What is not known is the regulation that turns on the *lin-4* transcription in late L1.

The onset of *lin-4* expression in late L1 is likely linked to the nutritional state. *C. elegans* needs to feed to initiate the post-embryonic developmental programs of the L1 stage. When newly hatched animals encounter an environment without food, they enter into a diapause state in which development is suspended, and they become more resistant to environmental stress. In the case of epidermal blast cell division, the cycling inhibitors are promoted by more activated FOXO transcription factor DAF-16 due to starvation, which suppresses the blast's division[29, 30]. During L1 diapause, *lin-4* expression is suppressed, but this suppression is largely independent of *daf-16*[30], suggesting that *lin-4* expression onset during mid-late L1 under nutrient-rich environment is not a result of simple attenuation of *daf-16* activity. It is worth noting that external food signals are insufficient to drive *lin-4* expression as *lin-4* doesn't promptly turn on when animals encounter food. Therefore, *lin-4* expression must reflect the combination of the decision of the internal nutritional state and developmental progression.

Another unique developmental event that occurs at late L1 is the synaptic rewiring of DD motor neurons[21, 31, 32]. The process enables a structural and functional switch between dendritic

and axonal domains of DDs without an obvious transition in gross neuronal morphology. We previously identified the membrane-bound transcription factor MYRF-1 as an essential positive regulator of synaptic rewiring in DDs[33]. MYRF-1 is broadly expressed, and *myrf-1* loss of function results in animals being arrested at the end of L1 or during L2. Intriguingly, the MYRF-1 protein is localized on the cell membrane during early and mid-L1 but increasingly undergoes self-cleavage towards late L1 in response to unidentified signaling mechanisms[34]. The enzymatic reaction of cleavage is expected to occur after trimerization of full-length MYRF-1, which releases N-MYRF-1 in trimeric form[35, 36], but the regulatory mechanisms underlying the process are unclear. Although MYRF-1's essential role in regulating the development of animals (including humans) is well-established[37-39], the functional targets of MYRF-1 remain elusive. In the course of studying the genetic interaction between *myrf-1* and *lin-14*, we discovered that MYRF-1 is required for *lin-4* expression. We present data demonstrating that MYRF-1 is a direct, cell-autonomous driver of *lin-4* expression.

Results

MYRF-1 is required for *lin-4* upregulation

The accumulation of *lin-4* microRNA occurs during mid to late L1, primarily due to an upregulation of transcription in *lin-4* primary RNA, as supported by multiple studies [25, 28](Figure 1A, C). We confirmed their findings by observing a P*lin-4*::*GFP* (*maIs134*) reporter generated by Ambros group[28], consisting of 2.4 kb of DNA sequences upstream of the mature *lin-4* fused to GFP. After its on-set, *lin-4* expression appears to constitutive and ubiquitous throughout the larval stages (see discussion). MYRF-1 is also expressed broadly in larvae, but unlike *lin-4*, MYRF-1 transcription is active in both embryos and early L1, with an increase in transcription observed towards late L1[33]. However, the activity of MYRF-1 as a transcription factor is determined by the presence of N-MYRF-1 in the nucleus[34]. Initially, full-length MYRF-1 localizes to the cell membrane during early L1, and only during mid to late L1 is the processing of MYRF-1 cleavage

increased, resulting in an elevated amount of N-MYRF-1 being released and shuttled into the nucleus (Figure 1A, B). Therefore, the nuclear accumulation of N-MYRF-1 coincides with the upregulation of *lin-4* both temporally and spatially.

The mutation *ju1121*(*G274R*) in the MYRF-1 protein not only abolishes its DNA binding capability but also negatively interferes with its close paralogue MYRF-2, resulting in *myrf-1(ju1121)* displaying phenotypic resemblance to double mutants of *myrf-1* and *myrf-2*[33]. Animals with the *myrf-1(ju1121)* mutation exhibit developmental arrest at L2 and eventually perish during L2-L3 molting. We find that *lin-4* transcription reporter fails to be upregulated in *myrf-1(ju1121)* at any viable stages that can be analyzed (Figure 2A, B). Similarly, another two loss of function mutants of *myrf-1*(*syb1468*) and *myrf-1*(*syb1491*) also shows a lack of *lin-4* transcription reporter signals (Figure S1A, B). Therefore, according to the 2.4 kb promoter reporter analysis, it is evident that the upregulation of *lin-4* is dependent on the presence of MYRF.

To confirm the crucial role of MYRF in the upregulation of *lin-4* transcription during late L1 stage, we investigated how myrf influences *lin-4* transcription by employing a reporter system with a nuclearly localized mScarlet protein, endogenously inserted at the *lin-4* locus (*umn84*), wherein the reporter open reading frame replaced the primary RNA sequence of *lin-4*. Our observations revealed that mScarlet signals were not detected in embryos and early L1 larvae ((Figure 2C, Figure 5A). However, these signals were significantly upregulated during late L1 stage and exhibited even stronger intensity in early L2 stage. Notably, in *myrf-1(ju1121)* mutants, the mScarlet signals were largely absent throughout the body during late L1 stage (14h), except for an interesting presence in 8-9 nuclei in the posterior bulb of the pharynx, with intensity comparable to that observed in the wild-type counterparts (Figure 2C, D, Figure S1C). The overall absence of *lin-4* upregulation persisted in *myrf-1(ju1121)* mutants during early L2 stage (21h), except for the aforementioned subset of pharyngeal nuclei where the mScarlet signals increased, although the ascent was much weaker compared to the wild-type controls.

We carried out qPCR analysis using probes specifically targeting *lin-4* microRNA to examine endogenous *lin-4* expression in wild type and *myrf-1(ju1121)* mutants, and observed a significant reduction in the levels of mature *lin-4* microRNA in *myrf-1(ju1121)* mutants (Figure 2E). This decrease of mature *lin-4* microRNA has been further confirmed through microRNA sequencing analysis (Figure 7A). These findings, combined with the analysis of endogenous *lin-4* reporter, provide compelling evidence supporting the critical role of MYRF in the upregulation of *lin-4* during the late L1 stage.

To investigate if MYRF-1 is continuously required for *lin-4* transcription after its initial upregulation, we used the auxin-inducible degradation (AID) system[41]. We combined the ubiquitously expressed F-box protein TIR1 with degron-tagged MYRF-1 to acutely deplete MYRF-1 protein. The degradation was induced by treating animals at L2, L3, and L4 stages with an NAA solution, an auxin analog. Our results showed a significant reduction in the *lin-4* transcription reporter signals in animals of all tested stages within 10 hours' post-treatment (Figure S2). This demonstrates that MYRF-1 is necessary for *lin-4* expression throughout the larval stages.

Sustained high level of LIN-14 protein in *myrf-1* mutants

The LIN-14 protein is typically present in embryos and early L1 but is downregulated as development progresses. Loss of the microRNA *lin-4* leads to sustained high levels of LIN-14 protein throughout larval development[11]. To investigate how *myrf-1* mutations may affect LIN-14, we examined the signals of endogenously tagged LIN-14::GFP in *myrf-1(ju1121)* mutants[40]. The LIN-14::GFP signal remains bright and shows no signs of decreasing at late L1 and beyond in *myrf-1(ju1121)* mutants (Figure 3A, B), consistent with the low levels of *lin-4* microRNA observed in the mutants.

MYRF-1 regulates *lin-4* expression cell-autonomously

Although MYRF is essential for larval development, there is limited understanding of how MYRF specifically affects tissues and cells during development. Identifying *lin-4* as a potential transcriptional target of MYRF-1, we aimed to investigate how MYRF-1 may regulate *lin-4* transcription. The primary question is whether MYRF-1 promotes *lin-4* expression in target cells or whether MYRF-1 acts to modify unidentified systemic signals that subsequently lead to upregulation of *lin-4* in terminal cells.

We conducted tissue-specific rescue experiments by expressing MYRF-1 under the *myo-3* promoter, which is specific to body wall muscles, in *myrf-1(ju1121)* mutants. We observed a significant induction of *lin-4* transcription in body wall muscles but not in other tissues (Figure 4A). We also used the epidermis-specific promoter of *dpy-7*, a collagen, for another MYRF-1 rescue experiment, which resulted in the appearance of *lin-4* transcription reporter signals only in the epidermis. Interestingly, the reporter GFP signals were not detected in the seam cells, a group of specialized epidermal cells embedded in the large syncytium epidermal hpy7 cell. Seam cells are derived from the epidermal lineage and also express the *dpy-7* gene; however, this experiment used a short promoter of *dpy-7*, which is not activated in seam cells, thus excluding the induction of *lin-4* in these cells. These results demonstrate that MYRF regulates *lin-4* transcription autonomously within specific cells.

One possible explanation for the deficiency of *lin-4* upregulation in *myrf-1(ju1121)* mutants is that it may be due to overall developmental arrest in L2. To investigate this possibility, we generated a conditional allele of *myrf-1*^{LoxP}(*ybq98*) using CRISPR-Cas9 editing. We then obtained an epidermis-specific Cre-expressing transgene and combined it with the *myrf-1*^{LoxP} allele in animals (Figure 4B, C). Our analysis showed that the *lin-4* transcription reporter signals in the epidermis are lost in animals with the combined Cre transgene and *myrf-1*^{loxP} allele, while the signals were

still present in all surrounding tissues. These results provide further evidence that MYRF-1 promotes *lin-4* upregulation cell autonomously and suggest that MYRF-1 acts directly in terminal tissues to regulate cell development.

Hyperactive form of MYRF-1 drives premature expression of *lin-4*

The next question was whether MYRF-1 is sufficient to drive the upregulation of *lin-4*. Because of the intricate nature of regulated MYRF-1 cleavage, overexpressing full-length MYRF-1 by transgene does not enhance its transcriptional activity effectively, as excess MYRF-1 is unable to traffic to the cell membrane or undergo adequate cleavage[33]. Overexpressing N-MYRF-1 alone is also insufficient as it unlikely forms trimers efficiently. In another study, we have identified elements of the cleavage mechanism, which we will report in another manuscript. Using this information, we created a truncated form of MYRF-1 (deleting 601-650) that is expected to bypass the need for cell-membrane trafficking and circumvent the developmental signals that control cleavage. We expected that overexpressing this modified MYRF-1 would produce abundant N-MYRF-1 in trimeric form and enhance its endogenous function.

In this experiment, we used the endogenously mScarlet-tagged line to report the transcription activity of *lin-4 (umn84)*. As mentioned earlier, mScarlet expression is not detected in embryos and early L1 larvae (Figure 2C, Figure 5A). We find that overexpressing the hyperactive MYRF-1(Δ601-650) driven by the ubiquitous promoter *rpl-28* is detrimental to larval development, as all F1 progenies with the transgene arrest at early larval stages. Strikingly, expressing this hyperactive MYRF-1 variant causes upregulation of *lin-4* transcription reporter in both embryos and early L1 larvae, indicating that MYRF-1 alone is sufficient to activate *lin-4* transcription (Figure 5B). Given that *lin-4* transcription is suppressed by FLYWCH during embryogenesis and by distinct yet unidentified mechanisms during early L1, MYRF-1 may play a predominant role in promoting *lin-4* transcription.

In our previous study, we characterized a mutant of *myrf-1*$^{1\text{-}700}$*(syb1313)* that exhibited precocious synaptic remodeling and M-cell division during mid-late L1, albeit in a discordant manner[34]. Our analysis of MYRF-1$^{1\text{-}700}$ localization led us to infer that MYRF-1(syb1313) functions as a constitutively active protein in specific cell types, but weakly and inconsistently. In the current study, we investigated the expression of the *lin-4* transcription reporter in *myrf-1(syb1313)* and observed a clear upregulation of the reporter in the mutants, especially in neurons, at 6 hours, while it was undetectable in wild-type animals at this stage (Figure 5C, D). It is worth noting that at the time (15h) when *lin-4* is typically upregulated in wild-type animals, the reporter GFP expression is significantly absent in the pharynx and epidermis of *myrf-1(syb1313)* mutants. However, there is sustained, higher-than-wild type expression of the reporter GFP in neurons of these mutants. Considering the precocious phenotype observed in DD neurons in *myrf-1(syb1313)*, these data support that hyperactive MYRF-1 promotes the premature transcription of *lin-4*.

We conducted further analysis to investigate the impact of *myrf-1*$^{1\text{-}700}$*(syb1313)* on the endogenously tagged mScarlet *lin-4* transcription reporter. In the mutants, we observed premature upregulation of mScarlet signals in a subset of nuclei, likely neurons based on their position and nucleus size, at 6 hours (Figure 5E, F). As mutant animals progressed towards late L1 (14h), the signal intensity significantly increased and remained consistently higher compared to the wild type controls. From this stage on, while the mScarlet signals in many wild type individuals were still in the process of upregulation, the signal intensity in *myrf-1*$^{1\text{-}700}$*(syb1313)* mutants did not exhibit a comparable sustained increase. This observation aligns with our assessment of *myrf-1*$^{1\text{-}700}$*(syb1313)* mutants, indicating an inconsistent precocity and developmental progression deficiency. Nonetheless, these results strongly support the notion that hyperactive MYRF can precociously activate endogenous *lin-4* transcription.

It is worth noting that in *myrf-1*$^{1-700}$*(syb1313)* mutants, the mScarlet signals exhibit strong upregulation in a few nuclei located in the posterior bulb of the pharynx at 14 hours, in comparison to the wild type (Figure 5E, F). These cells appear to belong to the same subset, as determined by their position and pattern, where the mScarlet signals have not experienced a significant decrease as observed in many other neighboring cells when MYRF function is lost (Figure 2C, D). This result indicates that hyperactive MYRF indeed enhances *lin-4* transcription in this specific subset of pharyngeal cells. However, it is noticeable that at 6 hours, the mScarlet signals in these nuclei of *myrf-1*$^{1-700}$*(syb1313)* mutants are not as bright as nearby neurons, suggesting that MYRF-1$^{1-700}$ does not activate *lin-4* expression effectively in these pharyngeal nuclei at early L1.

The strong induction of mScarlet signals in these pharyngeal nuclei at late L1 and onwards in *myrf-1*$^{1-700}$*(syb1313)* mutants contrasts with the lack of *maIs134* signals in the pharynx of the mutants. One possible explanation for this contrasting expression pattern is the presence of additional pharynx-enhancing elements located outside the 2.4 kb promoter region of *lin-4* used in the *maIs134* transgene. Alternatively, it should be considered that the threshold for transcription factor activation required to drive the expression of the endogenous reporter (mScarlet) versus the multicopy DNA array reporter (*maIs134*) is likely different. Therefore, resolving this discrepancy would require further investigation.

MYRF-1 interacts with *lin-4* promoter directly

We next investigated whether MYRF-1 physically binds to *lin-4* regulatory sequences to regulate *lin-4* transcription. Gel mobility shift assays are commonly used to test the direct interaction between protein and DNA fragments. A series of MYRF-1 variants were expressed in HEK cells by transfection, and cell lysis was tested for their binding with 498 bp DNA of the *lin-4* promoter. None of the *C. elegans* MYRF-1 variants including full-length and N-MYRF-1$^{1-482}$ display significant binding with 498 bp *lin-4* promoter. This negative result is difficult to interpret

considering when *C. elegans* MYRF-1 is expressed HEK cell lines, they do not assemble into trimer nor be cleaved (while mammalian MYRF does) for unknown reasons[33], which may render them incompetent to bind target DNA.

While analyzing *Plin-4-GFP(maIs134)*, we observed that the multicopy transgene of *lin-4* promoter DNA caused unexpected developmental abnormalities in animals. Previously, we used combined alleles, *myrf-1(ju1121)* along with a rescuing multicopy transgene *myrf-1*^{LoxP}(*ybqIs112*) for the conditional ablation of *myrf-1*[33]. In our current study, we introduced the *Pdpy-7-Cre* transgene into the combined-conditional *myrf-1* alleles (*ju1121-ybqIs112*) to examine *maIs134* expression in the epidermis where *myrf-1* is to be ablated. We observed a certain percentage of dauers emerging on plates even when the food *E. Coli* OP50 had not been exhausted (Figure 6A, B; Figure S3). Dauer refers to the alternative L3 stage that animals develop into when they encounter unfavorable living conditions such as low food abundance and high temperature. Because wild type *C. elegans* would never become dauer before the food runs out, this type of dauer formation is only associated with certain types of mutants, termed as the constitutive dauer formation (Daf-C). With intrigue, we initially thought that the dauer is due to the loss of *myrf-1* in the epidermis; however, the *maIs134* transgene animals themselves produce a low percentage of Daf-C, although the combinatorial effect of the conditional *myrf-1* alleles (*ju1121-ybqIs112*) and epidermal-Cre remains to be characterized. We also noticed that animals carrying *maIs134* invariably develop slower than wild-type animals, even though they show no obvious defect in becoming adults and in fertility (Figure 6B-F). The developmental delay starts from L2 and onwards based on their appearance and body length measurement. The L2 animals of *maIs134* are typically darker, longer, fatter than normal L2 animals and resemble pre-dauer (L2d) animals in gross morphology (Figure 6F). We interpret the Daf-C phenotype in *maIs134* with the reasoning that the transgene containing tandem array of *lin-4* promoter DNA sequestered a significant amount of the MYRF-1 protein, causing MYRF-1 to drop to such a low level that impedes normal development. A salient phenotype of *myrf-1* mutants is developmental arrest

after all. If the hypothesis was true, expressing more MYRF-1 in *maIs134* animals might suppress the Daf-C phenotype. In the rescuing transgene *myrf-1*^{LoxP}(*ybqIs112*) MYRF-1 protein is expected to increase slightly more than its endogenous level. This notion is indeed consistent with the observation that *ybqIs112* transgene completely suppressed the slow-growth phenotype in *maIs134*, as well as the Daf-C (Figure 6A-D), suggesting that the transgene of *lin-4* promoter DNA negatively interferes with the normal function of MYRF-1 in development.

These observations prompted us to investigate further whether the transgene array of *lin-4* promoter DNA effectively binds a significant amount of MYRF-1 protein. To test this, we injected the *lin-4* promoter (498 bp or 2.4 kb) reporter plasmid into *myrf-1*^{GFP}(*ybq14*), and remarkably, we detected some puncta of intensified GFP signals in a subset of nuclei in animals carrying transgene (Figure 6G-I; Figure S4). This suggests that the MYRF-1^{GFP} protein is condensed in discrete nuclear locations, a phenomenon that we never observed in wild type *myrf-1*^{GFP}(*ybq14*) animals. To determine the specificity of their interaction, we designed a plasmid of *lin-4* promoter DNA without the sequence encoding RFP or GFP, and a second plasmid containing 7x TetO sequence to be bound by TetR. We generated a line of ubiquitously expressed TetR DNA binding domain fused with RFP (TetR::RFP) as a single copy transgene (*ybqSi233*) to ensure consistent expression of TetR::RFP at a moderate level (Figure 6G, H). The formation of the TetO tandem DNA array indeed led to the formation of TetR::RFP puncta, demonstrating the effectiveness of the method. The presence of RFP puncta can then mark the location of DNA arrays in the nucleus. The formation of the TetO DNA array alone was insufficient to sequester MYRF-1^{GFP}, while only the addition of the *lin-4* promoter DNA into the tandem array caused the emergence of the MYRF-1^{GFP} puncta, indicating the specificity of the *lin-4* promoter-MYRF-1 interaction. Therefore, the collection of serendipitous observations and the nuclear loci co-labelling *in vivo* supports the direct regulator role of MYRF-1 in driving *lin-4* transcription.

MYRF-1 regulates a selective subset of microRNAs during L1-L2 transition

We wanted to investigate the extent to which MYRF-1's transcriptional activity might affect the landscape of microRNA expression in genome, as microRNAs often have stronger effects when present in combination with homologous microRNAs or in synergy with other microRNA families[22]. We performed microRNA-targeted sequencing analysis on *myrf-1(ju1121)* mutants of late L1 (16 hours) compared to controls. The sequencing analysis showed that a small subset of microRNA species was differentially expressed between *myrf-1(ju1121)* and control animals ($P<0.05$) (Figure 7A). We performed a phylogenetic analysis to analyze the relationships between these microRNA species (Figure 7B). Remarkably, 6 out of the 7 up-regulated microRNAs are clustered on one phylogenetic branch, which is separate from the other two. Among the differentially expressed, *lin-4* was the most decreased gene, consistent with our present analysis on *lin-4*. We then selected several candidates of relative abundance and examined their expression using transcriptional reporters. We generated single copy insertion transgenes carrying 2 kb upstream sequences of the candidate microRNA and eventually obtained lines for *mir-48*, *mir-73*, and *mir-230* showing consistent GFP signals (Figure 7C, D). The *mir-48* reporter (*ybqSi206*) was decreased, while *mir-73* (*ybqSi208*) and *mir-230* (*ybqSi209*) were increased in *myrf-1(ju1121)* at early L2, thus confirming the microRNA sequencing results. Notably, all three microRNAs were increased from L1 to L2 by transcriptional reporter; among the three, *mir-48* reporter is hardly detected in L1 and shows the most dramatic upregulation when animals transition to L2. The loss of *myrf-1* significantly decreased *mir-48*'s upregulation, but did not completely block it as it did with *lin-4*. *mir-48* belongs to the *let-7* microRNA family, and two other family members, *mir-84* and *mir-241*, were also downregulated in *myrf-1(ju1121)*, while *let-7*, the founding member, itself was upregulated in the mutants. Among the microRNAs upregulated in the *myrf-1* mutants, *mir-42* belongs to the *mir-35* family, which is essential for embryogenesis, and *mir-71* has been extensively studied for its upregulation in adults and regulatory role in aging. At this stage, it is unclear how these candidate microRNAs may be involved in regulating post-

embryonic development, but our results suggest an intricate genetic circuit in which MYRF-1's activity may either enhance or dampen the expression of select microRNA species.

Discussion

Our study reveals that the nuclear accumulation of released N-terminal MYRF-1 increases from mid L1 to late L1, coinciding with the upregulation of *lin-4* expression. We demonstrated that MYRF-1 is essential for the upregulation of *lin-4* in terminal tissues in L1 and also required for *lin-4* expression throughout the larval stages (Figure 7E). Our data support the direct, predominant role of MYRF-1 in driving *lin-4* transcription.

While *lin-4* expression appears to be constitutive after late L1 by stable GFP reporter, the analysis with higher temporal resolution showed that it exhibits oscillation in each larval stage[42, 43]. The periodic activation of *lin-4* transcription is likely driven by poorly understood oscillation gene regulatory circuits, some of which include *C. elegans* orthologs of human circadian clock genes[44-49]. Recent work has begun to reveal the regulation mechanisms underlying oscillating *lin-4* transcription[43, 49, 50]. BLMP-1/PRDM1 functions as a nutrient-stimulated priming factor to decompact the *lin-4* locus and boost the amplitude of *lin-4* oscillation[43]. It is worth noting that the expression of BLMP-1 itself does not oscillate. However, two other oscillating nuclear hormone receptors, NHR-85/Rev-Erb and NHR-23/ROR, promote *lin-4* transcription, ensuring its precise oscillation timing[50]. These two receptors are the closest nematode orthologs of human circadian transcription factors Rev-Erb and ROR, respectively. The expression of NHR-85 is downregulated post-transcriptionally by LIN-42/PERIOD, another ortholog of the human circadian factor[50]. LIN-42/PERIOD peaks in each cycle, but lags behind NHR-85 and NHR-23. Although the interactions between BLMP-1, NHR-85, and NHR-23 constitute an attractive model for explaining the oscillation of *lin-4* expression, it remains unclear to what extent the upregulation of *lin-4* expression, particularly during late L1, relies on these factors. For instance, there is a lack of

description regarding the impact of BLMP-1, NHR-85, and NHR-23 mutants on endogenous *lin-4* expression. Exploring how MYRF-1 interacts with the three components of *lin-4* oscillation control—BLMP-1, the NHR-85 and NHR-23 pair, and LIN-42—would be an interesting direction for further study.

Similar to the orthologs of circadian genes, *myrf-1* mRNA exhibits oscillation in each larval stage as part of an oscillation scheme consisting of over 3000 genes oscillating at specific phases in each cycle[44, 45]. These gene expression patterns, including *lin-4*, are halted during acute food removal/starvation, indicating that cycle progression is regulated by nutritional state[43, 51]. Our report includes the partial dauer-constitutive phenotype caused by the interaction between the *lin-4* promoter DNA and MYRF-1. Although we do not fully understand the phenomenon, it clearly points to a link between MYRF-1 activity and nutrient state. Investigating how MYRF-1 responds to nutrient signals, what transcriptional outcome it produces, and its position in the regulatory circuit of oscillation will be important topics for future investigation.

Materials and Methods

Animals

Wild-type C. elegans were Bristol N2 strain. Strains were cultured on NGM plates using standard procedures (Brenner, 1974). Unless noted, animals were cultured at 20°C for assays requiring specific developmental stages. Animals analyzed in this paper were hermaphrodite

Naming of the Alleles

All alleles generated in Y.B.Q. lab are designated as "ybq" alleles, and all strains, as "BLW" strains. "Ex" denotes transgene alleles of exchromosomal array. "Is" denotes integrated transgene. "Si" denotes single-copy integrated transgene. "syb" alleles (in "PHX" strains) are generated by genomic editing using CRISPR-Cas9 technique. "syb" alleles were designed by Y.B.Q. and produced by SunyBiotech (Fuzhou, China).

myrf-1 alleles by CRISPR-Cas9 editing

For the following described alleles generated by CRISPR-Cas9 editing,

Cas9 and gRNA were expressed from plasmids. The positive clones were identified using PCR screening to test singled F1 resulted from microinjection. GFP::myrf-1(LoxP) (ybq98) alleles was generated in the background of strain BLW889 [GFP::myrf-1::3xFlag(ybq14)]. Two artificial introns are inserted into the third exon of myrf-1 gene and each intron carries one LoxP site.

gRNA target: sgRNA1: TCAAGTCGGCTTCTCTTACGTGG

sgRNA2: TACGTGGCATCTCCAAAACAGGG

ybq14(background): …GGAATGCCAAGCCCTGTTTTGGAGATGCCACGTAAG - (insertion point) -

AGAAGCCGACTTGACACCCCGTGTGAAACGCCAAGAATCGCTCCAAGCTTTGCTGGTATTG

ACGGATTTCCAGATGAGAATTACAGTCAGCAACAGGCAATCAG - (insertion point) -

ATTCTCAAAGTTTCAAGAAGAACAGTGGAGTCCACTGTATGACATCAACGCTCAACCGCTAC

AACAACTTCAA...

ybq98: …GGAATGCCAAGCCCTGTCTTAGAAATGCCACGCAAG -

(gtatgtttcgaatgatactaataATAACTTCGTATAGCATACATTATACGAAGTTATaacataacatagaacattttc

ag) –

AGAAGCCGACTTGACACCCCGTGTGAAACGCCAAGAATCGCTCCAAGCTTTGCTGGTATTG

ACGGATTTCCAGATGAGAATTACAGTCAGCAACAGGCAATCAG -

(gtaagtttaaactttctcatactaataATAACTTCGTATAGCATACATTATACGAAGTTATattaactaacgcgctcta

tttaaattttcag) –

ATTCTCAAAGTTTCAAGAAGAACAGTGGAGTCCACTATACGATATTAACGCTCAACCGCTACA

ACAACTTCAA...

GFP::Degron::myrf-1::3xFlag(ybq133) was generated in the background of BLW889 [GFP::myrf-1::3xFlag(ybq14)]. Degron is inserted after the last amino acid of GFP (Lys).

sgRNA: CAATCAACCTACAAACACCCTGG

ybq14(background): …GGGATTACACATGGCATGGATGAACTATACAAA - (insertion point) – GCAGTCAATCAACCTACAAACACCCTGGCTCAACTCAA...

ybq133: …GGGATTACACATGGCATGGATGAACTATACAAA - DEGRON GCAGTCAATCAACCTACAAACACCCTTGCTCAACTCAA...

Generation of transgene alleles

Pmyo-3-MYRF-1 transgene: The vector pQA1094 [Pmyo-3-myrf-1] was injected to BLW1424 [myrf-1(ju1121)/mIn1 II; lin-4p::GFP+unc-119(maIs134)] at concentration of 0.5 ng/µl. The resulting strain is BLW1579 [myrf-1(ju1121)/mIn1 II; lin-4p::GFP+unc-119(maIs134); Pmyo-3-myrf-1(ybqEx746)]

Pdpy-7-MYRF-1 transgene: The vector pQA1511 [Pdpy-7-gfp::myrf-1] injected to N2 at concentration of 0.5 ng/µl to generate BLW1562 [Pdpy-7-gfp::myrf-1(ybqEx721)]. ybqEx721 was crossed into VT1072 [unc-119(ed3) III; lin-4p::GFP+unc-119(maIs134)] to generate BLW1578 [lin-4p::GFP+unc-119(maIs134); Pdpy-7-gfp::myrf-1(ybqEx721)]. BLW1578 was crossed with BLW1424 [myrf-1(ju1121)/mIn1 II; lin-4p::GFP+unc-119(maIs134)] to generate BLW1580 [myrf-1(ju1121)/mIn1 II; lin-4p::GFP+unc-119(maIs134); Pdpy-7-gfp::myrf-1(ybqEx721)].

Overexpress GFP::MYRF-1 (delete 601-650): The vector pQA1922[Prpl-28-GFP::myrf-1(delete 601-650)] were injected into CGC177[lin-4(umn84[lin-4p::SL1::EGL-13NLS::lox2272::mScarlet-I::cMycNLS::Lox511I::let-858-3'UTR::lox2722])/mIn1[dpy-10(e128) umnIs33] at 10 ng/µl.

Tandem DNA array of Plin-4(2412 bp) DNA: The vector pQA1881 [Plin-4(2412bp) -unc-54-3'UTR] was injected into BLW1827 [gfp::myrf-1](ybq14); glo-1(zu391)] at 50 ng/µl.

Tandem DNA array of Plin-4(498bp) DNA: The vector pQA1880 [Plin-4(498bp) -unc-54-3'UTR] was injected into BLW1827 [gfp::myrf-1](ybq14); glo-1(zu391)] at 50 ng/µl.

Tandem DNA array of 7xTetO: The vector pQA1961 [7xTetO] was injected into BLW2170 [gfp::myrf-1(ybq14)]; glo-1(zu391); Prpl-28-TetR-DBD::TagRFP(ybqSi233)] at 50 ng/µl.

Tandem DNA array of Plin-4 DNA+7xTetO: The vector pQA1960 [Plin-4(2412bp) -unc-54-3'UTR -7xTetO] were injected into BLW2170 [gfp::myrf-1(ybq14)]; glo-1(zu391); Prpl-28-TetR-DBD::TagRFP(ybqSi233)] at 50 ng/µl.

Pmir-48-gfp single copy transgene: The pQA1861 [Pmir-48-GFP miniMos_vector] at 50 ng/µl and standard components of miniMos system (see below) was injected into N2 animals to make single copy transgene Pmir-48-GFP(ybqSi206).

Pmir-73-gfp single copy transgene: The pQA1863 [Pmir-73-GFP miniMos_vector] at 50 ng/µl and standard components of miniMos system (see below) was injected into N2 animals make single copy transgene Pmir-73-GFP(ybqSi208).

Pmir-230-GFP single copy transgene: The pQA1864 [Pmir-230-GFP miniMos_vector] at 50 ng/µl and standard components of miniMos system (see below) was injected into N2 animals make single copy transgene Pmir-230-GFP(ybqSi209).

TetR-TagRFP single copy transgene: The pQA1896 [Prpl-28-TetR-DBD::TagRFP miniMos_vector) at 50 ng/µl and standard components of miniMos system (see below) was injected into N2 animals make single copy transgene Prpl-28-TetR::TagRFP (ybqSi233).

Single-copy integrated transgene allele

The procedure for generating single-copy integrated transgenes using miniMos technology in this study followed the protocol established by Frøkjær-Jensen et al. (2014). The injection mixture contained 10 ng/µl pGH8 [Prab-3::mCherry], 2.5 ng/µl pCFJ90 [Pmyo-2::mCherry], 50 ng/µl pCFJ601 [Peft-3-Mos1-transposase], and 50 ng/µl miniMos plasmid harboring the target gene. The mixture was injected into the gonads of N2 animals. After injection, the nematodes were transferred onto NGM medium and incubated at 25°C for approximately 48 hours. Subsequently, 500 µl of 25 mg/mL G418 solution was added to each plate to screen for nematodes carrying the target transgene. After 7-10 days, healthy nematodes without mCherry co-markers were selected from the medium where all the food was consumed. Candidate single-copy integrators were grown on G418-containing plates and analyzed for target protein expression. Homozygous nematodes carrying a single-copy transgene were identified by their 100% resistance to G418 toxicity and expression of the target protein.

Taqman real time PCR analysis for miRNA lin-4

Samples for Taqman Real-Time PCR Assays were prepared from wild type N2 and BLW252 [myrf-1(ju1121)/mIn1] strains at three stages: Early L1 (0h), Late L1 (16h), and Early L2 (21h). The worms were screened for size and fluorescence marker of the desired transgene using Biosorter. myrf-1(ju1121) mutants lack the pharyngeal GFP, which serves as a transgene marker of balancer mIn1, as a criterion in sorting process. More than 2,000 worms were collected for each sample after the Biosorter process.

RNA extraction was carried out using RNAiso Plus (TaKaRa, Dalian, China) following the manufacturer's instructions with some modifications. Briefly, 1 ml of RNAiso Plus was added to each sample, which was homogenized using a pre-cooled grinder. The homogenization buffer was then transferred to a 1.5 ml microcentrifuge tube and allowed to stand at room temperature (15 – 30°C) for 5 – 10 min. The supernatant was discarded, and 200 µl of chloroform was added and shaken for 30 s until the mixture turned milky. The mixture was then centrifuged at 12,000g at 4°C for 15 min, and the supernatant was transferred to a new microcentrifuge tube. To the supernatant, 0.5 ml of isoamylol was added and left to stand for 10 min at room temperature, then centrifuged at 12,000g at 4°C for 60 min. After discarding the supernatant, the pellet was washed with 75% ethanol at 12,000g, 4°C for 60 min, and then dissolved in 20 µl of DEPC-treated water. The concentration of miRNA was determined using Nanodrop, and its quality was assessed through electrophoresis. Each experiment was performed using at least three replicates.

The TAKARA RNA reverse transcription kit (6110A) was used to perform RNA reverse transcription following the manufacturer's instructions. The concentration of the resulting product was measured using Nanodrop, and its quality was evaluated through electrophoresis.

The Taqman real-time PCR was conducted according to the Taqman small RNA assay protocol. Initially, the concentration of each sample was diluted to below 10 ng/µl, followed by reverse transcription PCR using the Taqman microRNA RT kit (4366596). Subsequently, the Taqman real-time PCR mixture was prepared using Taqman small RNA assay (20X) with lin-4a (21nt) (ID: 000258) and sn2323 (ID: 001760) as the internal control. Each sample was tested using at least

three technical replicates and three biological replicates. The Taqman real-time PCR was carried out using Applied Biosystems QuantStudio 7 Flex Real-Time PCR System (Thermofisher), and all the procedures were followed as per the instructions. To determine the relative changes of each sample in each assay, the lin-4 Ct of technical replicates was averaged and then subtracted by the average sn2323 Ct to obtain the △CT value for each sample. Within each biological replicate and assay, the difference between the △CT of each sample and the △CT of wild type at Early L1 was calculated to obtain △△CT. The 2 to the power of △△CT was then calculated to obtain the fold change in each sample compared to the wild type at Early L1. The fold changes were plotted in Figure 1.

miRNA sequencing and bioinformatics analysis

BLW53 [Phlh-8-GFP(ayIs6)] and BLW1555 [myrf-1(ju1121)/ mIn1; Phlh-8-GFP(ayIs6)] strains were utilized for sample preparation. To isolate myrf-1 mutants, late L1 stage worms were selected based on size and lack of pharyngeal GFP (a balancer mIn1 marker) using Biosorter. Over 10,000 worms were collected for each sample for further experimentation. Total RNA was extracted and assessed for quality and quantity using Nanodrop and Agilent 2100, respectively. Samples with a total quantity of 3-5 μg and high quality (RIN > 10) were selected for miRNA library construction. The miRNA libraries were established and sequenced by Novogene Technology Co., Ltd. (Beijing, China).

In this study, the C. elegans Assembly WBcel235/ce11 was used as the reference genome for bioinformatic analysis of the sequencing data. The reference genome and gene annotation database were obtained from the EMSEMBL database and used for downstream analysis. The sequencing data was initially assessed for quality using the software FASTQ, followed by alignment of each miRNA sequencing dataset independently to the reference genome using HiSAT2. Transcriptome from each RNA-sequencing dataset was then extracted using the StringTie software. Differential miRNA cluster analysis was performed to compare miRNA expression of control and myrf-1(ju1121) mutant using DESeq2. Data normalization was done using the TPM method, and the profiling differences between control and myrf-1(ju1121) mutant

were compared using "Fold Change" (FC). A P-value was assigned to each gene and adjusted using the Benjamini and Hochberg method. Genes with P_adj < 0.05 were considered differentially expressed.

Microscopic analyses and quantification

Live animals were anesthetized using 0.5% 1-Phenoxy-2-propanol in ddH_2O and mounted on 3% Agar gel pad. The animals were examined under x20, x40, or x60 oil objective on OLYMPUS BX63 microscope. The wide-field DIC or fluorescence images (single plane images or Z-focal stacks) were taken by a sCMOS camera (PrimΣ Photometrics camera (model 2) mounted on OLYMPUS BX63, which is driven by CellSens Dimension software (Olympus). Images of live animals were also acquired on Zeiss LSM880 with Airyscan. The thickness of the optical slices was typically 0.8 µm.

To quantify the patterns of GFP::MYRF-1, we acquired images of stage-synchronized animals using wide-field microscopy as described above. The same parameters were used, including the power of excitation light, an identical objective, exposure duration, and screen display setting. The acquired images were examined, and the patterns of GFP::MYRF were categorized based on the consistency of the signals observed at specific subcellular locations throughout the animal body. A "weak or unclear signal" means that either no clear signals are detected or there are some weak signals that are inconsistent throughout the animal body. We carried out three independent rounds of culture, imaging, and scoring, and the data were pooled and presented in percentage column graphs.

To quantify the general Plin-4-GFP(maIs134) transcriptional reporter fluorescence intensity, we opened each acquired image stack in ImageJ and selected a single slice with a focused pharynx for further analysis. A square with sides 20 pixels (3.25 µm) long was drawn to the pharynx isthmus. The intensity of the region of interest (ROI) was measured and presented as Mean ± SEM (t-test, *, $p<0.05$; **, $p<0.01$; ***, $p<0.001$; ****, $p<0.0001$).

To quantify the pharyngeal Plin-4-GFP(maIs134) transcriptional reporter fluorescence intensity in myrf-1(syb1491) and myrf-1(syb1468) mutants, we opened each acquired image stack in ImageJ

and selected a single slice with a focused pharynx bulb for further analysis. The posterior pharynx bulb was selected as the ROI. The intensity of the ROI was measured and presented as Mean ± SEM (t-test, *, p<0.05; **, p<0.01; ***, p<0.001; ****, p<0.0001).

To quantify the neuronal Plin-4-GFP(maIs134) transcriptional reporter fluorescence intensity in myrf-1(syb1491) and myrf-1(syb1468) mutants, we opened each acquired image stack in ImageJ and selected a single slice with a focused head nerve ring for further analysis. The dorsal nerve ring area was selected as the ROI. The intensity of the ROI was measured and presented as Mean ± SEM (t-test, *, p<0.05; **, p<0.01; ***, p<0.001; ****, p<0.0001).

To quantify the whole body lin-4p::nls::mScarlet(umn84) transcriptional reporter fluorescence intensity, the z-stack was maximally projected to produce a single image in ImageJ. The whole animal area was selected as ROI. The intensity of the ROI was measured and presented as Mean ± SEM (t-test, *, p<0.05; **, p<0.01; ***, p<0.001; ****, p<0.0001).

To quantify the pharyngeal lin-4p::nls::mScarlet(umn84) transcriptional reporter fluorescence intensity in myrf-1(ju1121) and myrf-1(syb1313) mutants, we opened each acquired image stack in ImageJ and selected a single slice with a focused pharynx bulb for further analysis. Two posterior pharynx bulb nuclei were selected as the ROI. The intensity of the ROI was measured and presented as Mean ± SEM (t-test, *, p<0.05; **, p<0.01; ***, p<0.001; ****, p<0.0001).

To quantify the neuronal lin-4p::nls::mScarlet(umn84) transcriptional reporter fluorescence intensity in myrf-1(ju1121) and myrf-1(syb1313) mutants, we opened each acquired image stack in ImageJ and selected a single slice with a focused nerve ring for further analysis. Several neuron nuclei were selected as the ROI. The intensity of the ROI was measured and presented as Mean ± SEM (t-test, *, p<0.05; **, p<0.01; ***, p<0.001; ****, p<0.0001).

To quantify the LIN-14::GFP fluorescence intensity, we opened each acquired image stack in ImageJ and selected a single slice with a focused head neurons for further analysis. The head region was selected as the ROI. The intensity of the ROI was measured and presented as Mean ± SEM (t-test, *, p<0.05; **, p<0.01; ***, p<0.001; ****, p<0.0001).

To generate the line plot of TetR::TagRFP and GFP::MYRF-1, we opened each acquired image stack from Zeiss Airyscan in ImageJ and selected a single slice with a focused TetR::TagRFP spot for further analysis. We drew a 2-pixel (~0.1 μm)-thick, 12 μm-long ROI line to cross the center of one bright TetR::TagRFP spot. The middle point of the ROI line was positioned at the center of the spot. We ran the "plot profile" program located in the Analyze menu and recorded plot data in the RFP and GFP channels, respectively. The final graph was generated in GraphPad Prism 8. Each plot line represented the intensity distribution across a single TetR::TagRFP spot from an independent cell.

To generate a multiple line plot of GFP::MYRF-1, each image stack acquired from Zeiss Airyscan was opened in ImageJ, and a single slice with a focused GFP::MYRF-1 spot was selected. When no obviously bright GFP::MYRF-1 spot was found in the set of image slices, we chose a slice with clearly focused GFP::MYRF-1 signals in nucleus. A 2-pixel (~0.1μm)-thick, 10μm-long ROI line was drawn to cross the center of the GFP::MYRF-1 punctum (or brightest nucleus signal as we could fine). We then ran the program "plot profile", located in the Analyze menu, to record the plot data in the GFP channel. The final graph was generated in GraphPad Prism 8. The maximum intensity position in the ROI line was defined as the "0" position in the X axis. Measurement points within two microns centered at the "0" position were graphed. Each plot line represented the intensity distribution across a single GFP::MYRF-1 spot from an independent cell.

To generate a line plot of epidermal Plin-4-gfp in epidermal knock-out MYRF-1 animals, each acquired image stack was opened in ImageJ and a single slice with a focused seam cell was selected for further analysis. A 2-pixel (~0.1μm) thick, 12μm-long ROI line was drawn to cross a seam cell in a ventral-to-dorsal direction. The middle point of the ROI line was positioned at the center of the seam cell. The data was recorded by the "plot profile" program located in the Analyze menu. The final graph was generated using GraphPad Prism 8. Each plot line represented the intensity distribution across a single seam cell from an independent animal.

For quantification of miRNA transcriptional reporter fluorescence intensity, each image stack was opened in ImageJ and a single slice with focused head was selected for further analysis. A circle

ROI with a diameter of 10 pixels (1.625 μm) was drawn in the head region. For the mir-48 and mir-73 reporter, a circle was drawn on the pharynx bulb. For the mir-230 reporter, a circle was drawn on the first seam cell in the head. The intensity of the ROI was measured and presented as Mean ± SEM (t test. *, $p<0.05$; **, $p<0.01$; ***, $p<0.001$; ****, $p<0.0001$).

Assay of dauer formation with 1% SDS

To assay dauer formation, approximately 30 gravid adults (aged ~60 hours) were transferred to a fresh 3.5cm NGM plate where they laid eggs for four hours. Afterward, all adults were removed, and the synchronized eggs were maintained at 25℃ for 50 hours. To analyze the ratio of dauer formation, animals were washed from the NGM plate and treated with 1% SDS for 20 minutes. Surviving animals were counted and considered as dauer, while dead animals were counted and considered as non-dauer.

Assay of L2d formation by imaging

To assay L2d formation, approximately 30 gravid adults (aged ~60 hours) were transferred to a fresh 3.5cm NGM plate where they laid eggs for four hours. Afterward, all adults were removed, and the synchronized eggs were maintained at 20℃ for 48 hours. To analyze the morphology of animals, DIC images of animals were acquired on an OLYMPUS BX63 microscope using a x10 objective. Animals exhibiting a leaner morphology and more condensed intestinal granules were counted and considered as L2d.

Assay of dauer formation by imaging

To assay dauer formation, synchronized fresh-hatched L1 were seeded at ~200 per 3.5cm NGM plate and cultured at 20℃ for 70 hours. To analyze the morphology of animals, DIC images of animals were acquired on an OLYMPUS BX63 microscope using a x10 objective. Animals exhibiting a leaner and darker morphology were counted and considered as dauer.

Quantification of animal length

To quantify animal length and analyze their growth, DIC images of animals were acquired on an OLYMPUS BX63 microscope using a x10 objective. The lengths of animals in the images were

measured using the polyline tool in OLYMPUS imaging software, and the data were further analyzed in GraphPad Prism.

Auxin treatment

To perform auxin treatment, worms were transferred to OP50-seeded NGM plates containing ~4 mM K-NAA (1-Naphthaleneacetic acid potassium salt). Briefly, fresh OP50-seeded 3.5cm NGM plates with 3mL NGM agar and a 25mM K-NAA solution in ddH2O were prepared. Next, 500 μL of the 25mM K-NAA solution was added to the NGM plates and the lid was kept on until the solution dried. For all K-NAA treatment experiments, 500 μL of ddH2O was used as a control.

Phylogenetic analysis of differentially expressed miRNA genes

Phylogenetic analyses were performed using the MEGA 11.0 program. First, all miRNA sequences were imported into MEGA 11.0 and aligned using ClustalX to search for conserved bases and motifs. Pairwise distance was then estimated using the default parameters, except for the bootstrap replication number parameter, which was set to 1000, and the substitution model parameter, which was set to P-distance. The phylogenetic tree for our specific miRNAs was generated using the Neighbor-Joining method and default parameters, with branches corresponding to partitions reproduced in less than 0.1 bootstrap replicates filtered out.

Acknowledgments

Some strains were provided by the CGC, which is funded by NIH Office of Research Infrastructure Programs (P40 OD010440). We thank National Bioresource Project for *C. elegans* for providing some of the strains used in this study. This work was supported by the lab start-up fund from ShanghaiTech University to Y.B.Q.; by National Science Foundation for Young Scientists of China (grant no. 31900397) to L.W. We thank Xiaoting Feng for her assistance with the MYRF-1-AID experiments and Youzhe He at BGI-Shenzhen for providing bioinformatics support. We thank the Molecular and Cell Biology Core Facility (MCBCF) and the Molecular Imaging Core Facility (MICF) at the School of Life Science and Technology, ShanghaiTech University for providing technical support.

References

1. Wolpert, L., *Principles of development*. Sixth edition. ed. 2019, Oxford, United Kingdom ; New York, NY: Oxford University Press. xxiv, 741 pages.
2. Shi, Y.-B., *Animal metamorphosis*. 1st ed. Current topics in developmental biology,. 2013, San Diego, Calif.: Academic Press ;. xvi, 440 p., 14 p. of plates.
3. Truman, J.W., *Metamorphosis of the central nervous system of Drosophila.* J Neurobiol, 1990. **21**(7): p. 1072-84.
4. Huttenlocher, P.R., *Synaptic density in human frontal cortex - developmental changes and effects of aging.* Brain Res, 1979. **163**(2): p. 195-205.
5. Bethlehem, R.A.I., et al., *Brain charts for the human lifespan.* Nature, 2022. **604**(7906): p. 525-533.
6. Sun, H. and O. Hobert, *Temporal transitions in the postembryonic nervous system of the nematode Caenorhabditis elegans: Recent insights and open questions.* Semin Cell Dev Biol, 2023. **142**: p. 67-80.
7. White, J.G., et al., *The structure of the ventral nerve cord of Caenorhabditis elegans.* Philos Trans R Soc Lond B Biol Sci, 1976. **275**(938): p. 327-48.
8. White, J.G., et al., *The Structure of the Nervous System of the Nematode Caenorhabditis elegans.* Philos Trans R Soc Lond B Biol Sci, 1986. **314**(1165): p. 1-340.
9. Wood, W.B., *The Nematode Caenorhabditis elegans*. Cold Spring Harbor monograph series. 1988, Cold Spring Harbor, N.Y.: Cold Spring Harbor Laboratory. xiii, 667 p.
10. Ruvkun, G. and J. Giusto, *The Caenorhabditis elegans heterochronic gene lin-14 encodes a nuclear protein that forms a temporal developmental switch.* Nature, 1989. **338**(6213): p. 313-9.
11. Wightman, B., I. Ha, and G. Ruvkun, *Posttranscriptional regulation of the heterochronic gene lin-14 by lin-4 mediates temporal pattern formation in C. elegans.* Cell, 1993. **75**(5): p. 855-62.
12. Ambros, V. and H.R. Horvitz, *Heterochronic mutants of the nematode Caenorhabditis elegans.* Science, 1984. **226**(4673): p. 409-16.
13. Lee, R.C., R.L. Feinbaum, and V. Ambros, *The C. elegans heterochronic gene lin-4 encodes small RNAs with antisense complementarity to lin-14.* Cell, 1993. **75**(5): p. 843-54.
14. Ambros, V. and E.G. Moss, *Heterochronic genes and the temporal control of C. elegans development.* Trends in genetics : TIG, 1994. **10**(4): p. 123-7.
15. Rougvie, A.E. and E.G. Moss, *Developmental transitions in C. elegans larval stages.* Curr Top Dev Biol, 2013. **105**: p. 153-80.
16. Slack, F. and G. Ruvkun, *Temporal pattern formation by heterochronic genes.* Annu Rev Genet, 1997. **31**: p. 611-34.
17. Feinbaum, R. and V. Ambros, *The timing of lin-4 RNA accumulation controls the timing of postembryonic developmental events in Caenorhabditis elegans.* Dev Biol, 1999. **210**(1): p. 87-95.

18. Olsen, P.H. and V. Ambros, *The lin-4 regulatory RNA controls developmental timing in Caenorhabditis elegans by blocking LIN-14 protein synthesis after the initiation of translation.* Dev Biol, 1999. **216**(2): p. 671-80.
19. Howell, K., J.G. White, and O. Hobert, *Spatiotemporal control of a novel synaptic organizer molecule.* Nature, 2015. **523**(7558): p. 83-7.
20. Sun, H. and O. Hobert, *Temporal transitions in the post-mitotic nervous system of Caenorhabditis elegans.* Nature, 2021. **600**(7887): p. 93-99.
21. Hallam, S.J. and Y. Jin, *lin-14 regulates the timing of synaptic remodelling in Caenorhabditis elegans.* Nature, 1998. **395**(6697): p. 78-82.
22. Ambros, V. and G. Ruvkun, *Recent Molecular Genetic Explorations of Caenorhabditis elegans MicroRNAs.* Genetics, 2018. **209**(3): p. 651-673.
23. Akerblom, M., et al., *microRNA-125 distinguishes developmentally generated and adult-born olfactory bulb interneurons.* Development, 2014. **141**(7): p. 1580-8.
24. Boissart, C., et al., *miR-125 potentiates early neural specification of human embryonic stem cells.* Development, 2012. **139**(7): p. 1247-57.
25. Bracht, J.R., et al., *Regulation of lin-4 miRNA expression, organismal growth and development by a conserved RNA binding protein in C. elegans.* Dev Biol, 2010. **348**(2): p. 210-21.
26. Turner, M.J., A.L. Jiao, and F.J. Slack, *Autoregulation of lin-4 microRNA transcription by RNA activation (RNAa) in C. elegans.* Cell Cycle, 2014. **13**(5): p. 772-81.
27. Jiao, A.L., et al., *lin-4 and the NRDE pathway are required to activate a transgenic lin-4 reporter but not the endogenous lin-4 locus in C. elegans.* PLoS One, 2018. **13**(1): p. e0190766.
28. Ow, M.C., et al., *The FLYWCH transcription factors FLH-1, FLH-2, and FLH-3 repress embryonic expression of microRNA genes in C. elegans.* Genes Dev, 2008. **22**(18): p. 2520-34.
29. Baugh, L.R. and P.J. Hu, *Starvation Responses Throughout the Caenorhabditiselegans Life Cycle.* Genetics, 2020. **216**(4): p. 837-878.
30. Baugh, L.R. and P.W. Sternberg, *DAF-16/FOXO regulates transcription of cki-1/Cip/Kip and repression of lin-4 during C. elegans L1 arrest.* Curr Biol, 2006. **16**(8): p. 780-5.
31. White, J.G., D.G. Albertson, and M.A. Anness, *Connectivity changes in a class of motoneurone during the development of a nematode.* Nature, 1978. **271**(5647): p. 764-6.
32. Mizumoto, K., Y. Jin, and J.L. Bessereau, *Synaptogenesis: unmasking molecular mechanisms using Caenorhabditis elegans.* Genetics, 2023. **223**(2).
33. Meng, J., et al., *Myrf ER-Bound Transcription Factors Drive C. elegans Synaptic Plasticity via Cleavage-Dependent Nuclear Translocation.* Dev Cell, 2017. **41**(2): p. 180-194 e7.
34. Xia, S.L., et al., *The LRR-TM protein PAN-1 interacts with MYRF to promote its nuclear translocation in synaptic remodeling.* Elife, 2021. **10**.
35. Li, Z., Y. Park, and E.M. Marcotte, *A Bacteriophage tailspike domain promotes self-cleavage of a human membrane-bound transcription factor, the myelin regulatory factor MYRF.* PLoS biology, 2013. **11**(8): p. e1001624.
36. Kim, D., et al., *Homo-trimerization is essential for the transcription factor function of Myrf for oligodendrocyte differentiation.* Nucleic Acids Res, 2017.
37. Russel, S., A.R. Frand, and G. Ruvkun, *Regulation of the C. elegans molt by pqn-47.* Developmental biology, 2011. **360**(2): p. 297-309.

38. Emery, B., et al., *Myelin gene regulatory factor is a critical transcriptional regulator required for CNS myelination.* Cell, 2009. **138**(1): p. 172-85.
39. Huang, H., et al., *MYRF: A Mysterious Membrane-Bound Transcription Factor Involved in Myelin Development and Human Diseases.* Neurosci Bull, 2021. **37**(6): p. 881-884.
40. Arribere, J.A., et al., *Efficient marker-free recovery of custom genetic modifications with CRISPR/Cas9 in Caenorhabditis elegans.* Genetics, 2014. **198**(3): p. 837-46.
41. Zhang, L., et al., *The auxin-inducible degradation (AID) system enables versatile conditional protein depletion in C. elegans.* Development, 2015. **142**(24): p. 4374-84.
42. Kim, D., D. Grun, and A. van Oudenaarden, *Dampening of expression oscillations by synchronous regulation of a microRNA and its target.* Nat Genet, 2013. **45**(11): p. 1337-44.
43. Stec, N., et al., *An Epigenetic Priming Mechanism Mediated by Nutrient Sensing Regulates Transcriptional Output during C. elegans Development.* Curr Biol, 2021. **31**(4): p. 809-826 e6.
44. Hendriks, G.J., et al., *Extensive oscillatory gene expression during C. elegans larval development.* Mol Cell, 2014. **53**(3): p. 380-92.
45. Meeuse, M.W., et al., *Developmental function and state transitions of a gene expression oscillator in Caenorhabditis elegans.* Mol Syst Biol, 2020. **16**(7): p. e9498.
46. Tsiairis, C. and H. Grosshans, *Gene expression oscillations in C. elegans underlie a new developmental clock.* Curr Top Dev Biol, 2021. **144**: p. 19-43.
47. McCulloch, K.A. and A.E. Rougvie, *Caenorhabditis elegans period homolog lin-42 regulates the timing of heterochronic miRNA expression.* Proc Natl Acad Sci U S A, 2014. **111**(43): p. 15450-5.
48. Van Wynsberghe, P.M., et al., *The Period protein homolog LIN-42 negatively regulates microRNA biogenesis in C. elegans.* Dev Biol, 2014. **390**(2): p. 126-35.
49. Perales, R., et al., *LIN-42, the Caenorhabditis elegans PERIOD homolog, negatively regulates microRNA transcription.* PLoS Genet, 2014. **10**(7): p. e1004486.
50. Kinney, B., et al., *A circadian-like gene network regulates heterochronic miRNA transcription in C. elegans.* bioRxiv, 2023: p. 2022.09.26.509508.
51. Schindler, A.J., L.R. Baugh, and D.R. Sherwood, *Identification of late larval stage developmental checkpoints in Caenorhabditis elegans regulated by insulin/IGF and steroid hormone signaling pathways.* PLoS Genet, 2014. **10**(6): p. e1004426.

Figure 1

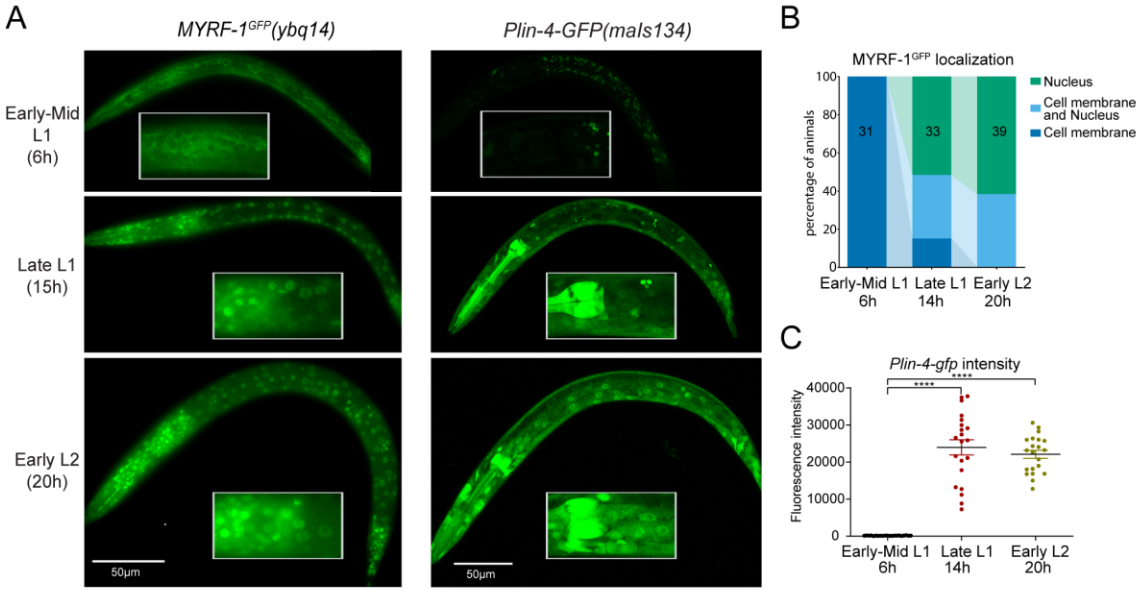
A
MYRF-1GFP(ybq14)
Plin-4-GFP(maIs134)
Early-Mid L1 (6h)
Late L1 (15h)
Early L2 (20h)
50µm
50µm
B
MYRF-1GFP localization
percentage of animals
100
80
60
40
20
0
31
33
39
Nucleus
Cell membrane and Nucleus
Cell membrane
Early-Mid L1 6h
Late L1 14h
Early L2 20h
C
Plin-4-gfp intensity
Fluorescence intensity
40000
30000
20000
10000
0
****
****
Early-Mid L1 6h
Late L1 14h
Early L2 20h

Figure 1. The nuclear accumulation of N-MYRF-1 coincides with the upregulation of *lin-4* in developmental timing.

A. Nuclear localization of GFP::MYRF-1 is increased in late L1, coinciding with the upregulation of *Plin-4-GFP*. GFP, endogenously inserted at MYRF-1 Ala171, labels both full-length MYRF-1 and post-cleaved N-MYRF-1. *Plin-4-GFP*(*maIs134*) is a transcriptional reporter of *lin-4*, carrying a 2.4 kb sequence upstream of the *lin-4* gene that drives GFP. While GFP::MYRF-1 is initially localized at the cell membrane in early-mid L1 (6 post-hatch hours), it becomes enriched in the nucleus towards late L1 (15 post-hatch hours). *Plin-4-GFP* is barely detected in early L1 but is upregulated in late L1. The insert shows a zoomed-in view of the framed area, covering part of the pharynx.

B. Quantification of animals showing a particular pattern of GFP::MYRF-1 (as shown in (A)) at various stages. The number of animals analyzed is indicated on each bar.

C. The fluorescence intensity of the *lin-4* transcriptional reporter (as shown in (A)) was quantified and presented as mean ± SEM (t-test, ****$p < 0.0001$); $n > 20$, where n is the number of nematodes analyzed.

Figure 2

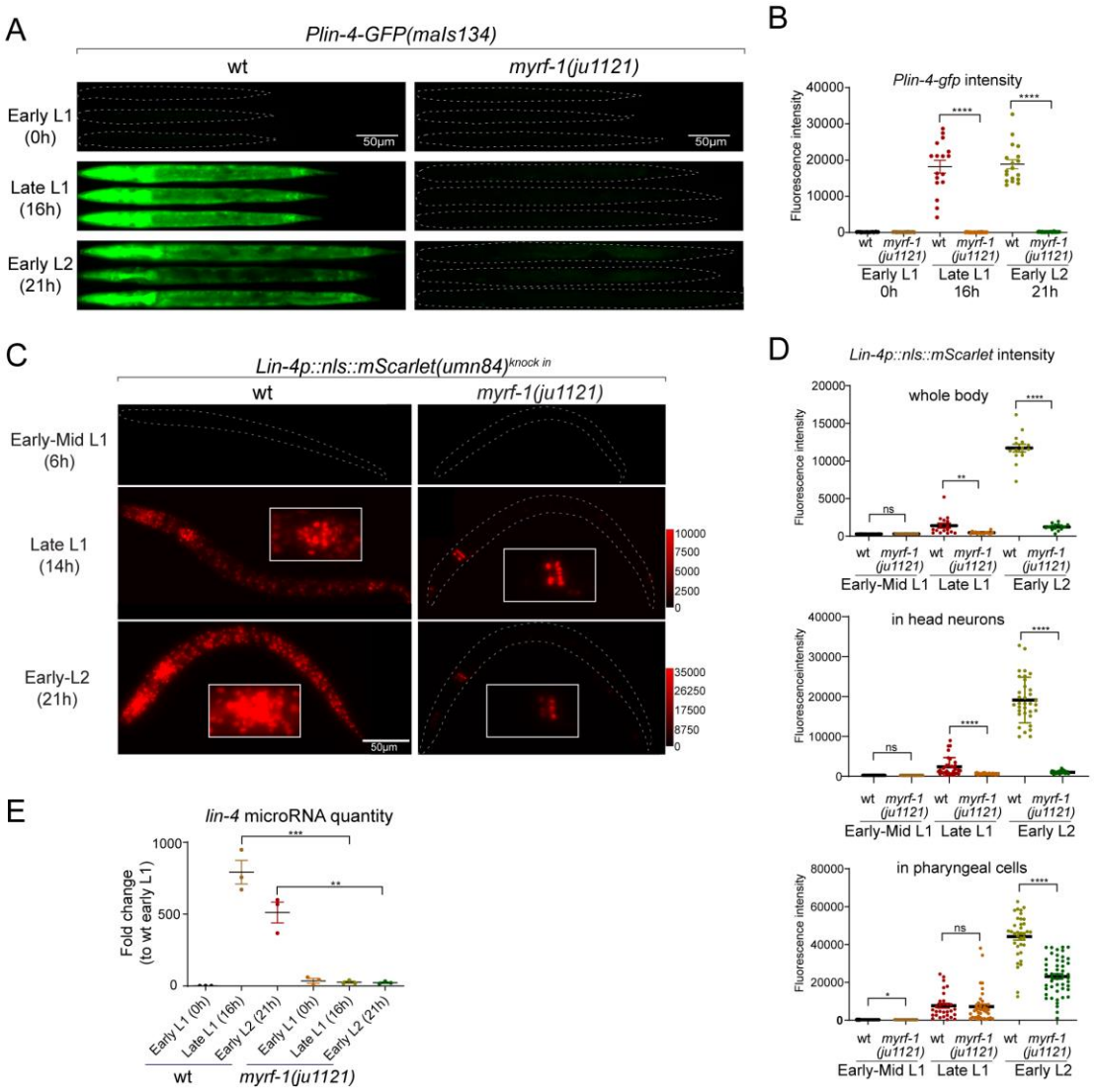
A
Plin-4-GFP(maIs134)
wt
myrf-1(ju1121)
Early L1 (0h)
Late L1 (16h)
Early L2 (21h)
50µm
B
Plin-4-gfp intensity
Fluorescence intensity
wt
myrf-1 (ju1121)
Early L1 0h
Late L1 16h
Early L2 21h
C
Lin-4p::nls::mScarlet(umn84)knock in
Early-Mid L1 (6h)
Late L1 (14h)
Early-L2 (21h)
D
Lin-4p::nls::mScarlet intensity
whole body
in head neurons
in pharyngeal cells
Early-Mid L1
Late L1
Early L2
E
lin-4 microRNA quantity
Fold change (to wt early L1)
Early L1 (0h)
Late L1 (16h)
Early L2 (21h)
wt
myrf-1(ju1121)

Figure 2. MYRF is required for *lin-4* upregulation during late L1

A. *Plin-4-GFP* is not upregulated in *myrf-1(ju1121)*. The expression of the *lin-4* transcriptional reporter in wild-type and *myrf-1(ju1121)* animals was examined at the early L1 (0h), late L1 (16h), and early L2 stages (21h).

B. The fluorescence intensity of the *lin-4* transcriptional reporter (as shown in (A)) was quantified and presented as mean ± SEM (t-test, ****$p < 0.0001$). More than 20 animals were analyzed.

C. The endogenous *lin-4* transcriptional reporter *lin-4p::nls::mScarlet(umn84)* is not upregulated in *myrf-1(ju1121)* except for a few pharyngeal nuclei. The expression of the *lin-4p::nls::mScarlet* in wild-type and *myrf-1(ju1121)* animals was examined at the early-mid L1 (6h), late L1 (14h), and early L2 stages (21h).

D. The fluorescence intensity of *lin-4p::nls::mScarlet(umn84)* (as shown in (C)) was quantified and presented as mean ± SEM (t-test, ****$p < 0.0001$). The "whole body" refers to the region of interest (ROI), which encompasses the entire body of the animal. The ROI of “in head neurons” comprises multiple head neuron nuclei found in each animal. For “in pharyngeal cells”, the ROI includes the 8-9 pharyngeal nuclei that exhibit bright mScarlet signals. More than 15 animals were analyzed.

E. The abundance of mature *lin-4* miRNAs in wild-type and *myrf-1(ju1121)* animals was examined at the early L1 (0h), late L1 (16h), and early L2 stages (21h) using qPCR analysis with probes specifically detecting *lin-4* microRNA. Each data point represents relative fold change of each sample comparing to the wild type Early L1 sample within one set of experiment. The data represent three biological replicates. Statistics used t-test. *$p < 0.05$, ***$p < 0.001$.

Figure 3

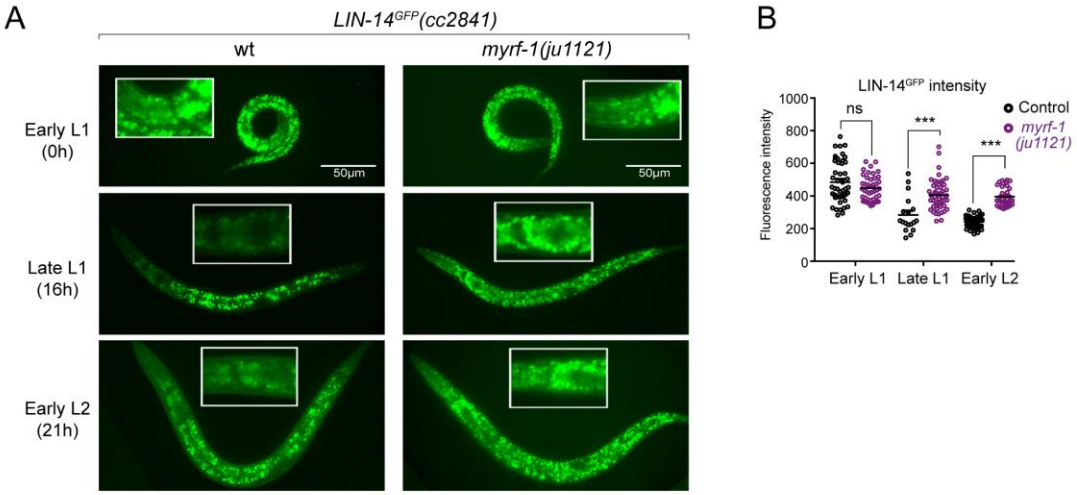
A
LIN-14GFP(cc2841)
wt
myrf-1(ju1121)
Early L1
(0h)
Late L1
(16h)
Early L2
(21h)
50µm
50µm
B
LIN-14GFP intensity
Fluorescence intensity
1000
800
600
400
200
0
ns
***
***
Control
myrf-1
(ju1121)
Early L1
Late L1
Early L2

Figure 3. There is a sustained high level of LIN-14 protein in *myrf-1* mutants.

A. Expression of LIN-14::GFP(*cc2841*) in wild-type and *myrf-1(ju1121)* at the early L1 (0h), late L1 (16h), and early L2 (21h) stages. GFP was endogenously tagged at the LIN-14 C-terminus. LIN-14::GFP is bright in early L1 and downregulated in late L1. LIN-14::GFP is not affected by *myrf-1(ju1121)* at early L1 but significantly brighter than wild-type control at late L1 and L2.

B: The fluorescence intensity for LIN-14::GFP (as shown in (G)) was measured and presented as mean ± SEM (t-test, ns: not significant, $p > 0.05$; ***: $p < 0.001$) from the analysis of more than 20 nematodes. Each data point represents the mean intensity of the head region in an individual animal. The head region was selected due to its low autofluorescence background

Figure 4

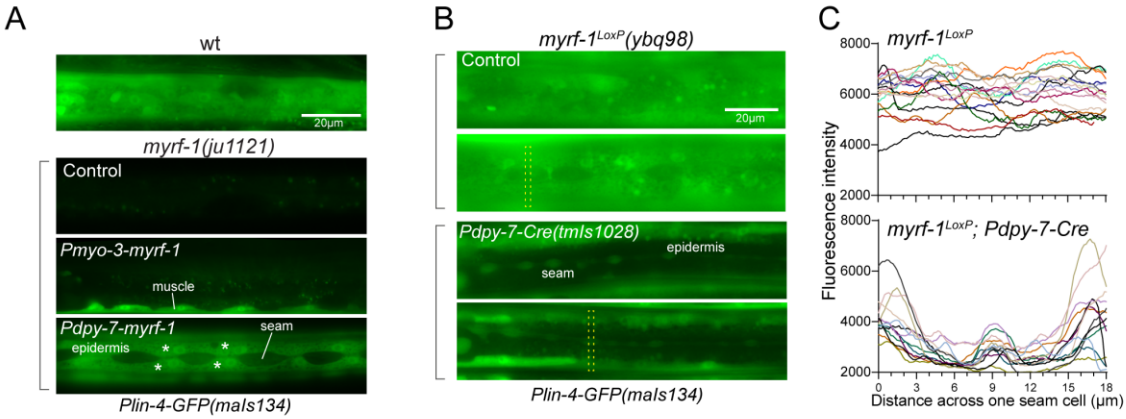
A
wt
20μm
myrf-1(ju1121)
Control
Pmyo-3-myrf-1
muscle
Pdpy-7-myrf-1
seam
epidermis
Plin-4-GFP(maIs134)
B
myrf-1LoxP(ybq98)
Control
20μm
Pdpy-7-Cre(tmIs1028)
epidermis
seam
Plin-4-GFP(maIs134)
C
myrf-1LoxP
myrf-1LoxP; Pdpy-7-Cre
Fluorescence intensity
8000
6000
4000
2000
0
3
6
9
12
15
18
Distance across one seam cell (μm)

Figure 4. MYRF-1 is sufficient to drive *lin-4* expression in a cell-autonomous manner.

A. Genetic rescue of MYRF-1 in *myrf-1*(*ju1121*) using tissue-specific promoters. *Plin-4-GFP(maIs134)* signals are observed specifically in body wall muscles and epidermis (asterisk) of *myrf-1*(*ju1121*) carrying transgene *Pmyo-3-myrf-1* and *Pdpy-7-myrf-1*, respectively, while no detectable *Plin-4-GFP* is observed in L2 of *myrf-1*(*ju1121*).

B. Tissue-specific ablation of *myrf-1* in the epidermis. *myrf-1*^{LoxP}*(ybq98)* combined with *Pdpy-7-NLS::Cre(tmIs1028)* caused loss or drastic decrease of *Plin-4-GFP*(*maIs134*) in the epidermis, while signals were detected in other tissues. Representative images of L2 (24h) animals are shown.

C. Fluorescence intensity measurements (as shown in (B)) are displayed for a ROI bar drawn transversely and centered at one seam cell. Individual lines represent signals from one animal.

Figure 5

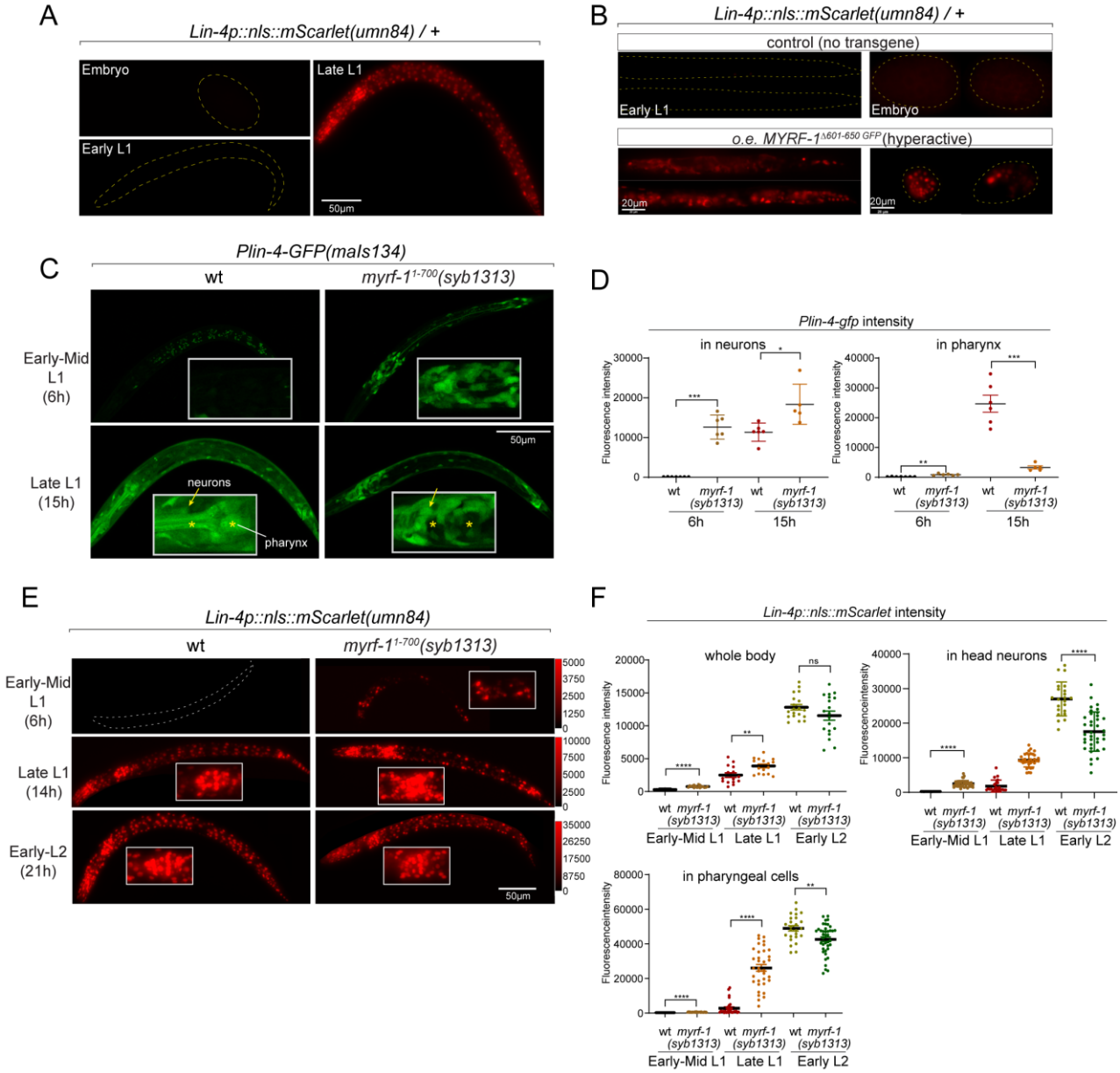
A
Lin-4p::nls::mScarlet(umn84) / +
Embryo
Early L1
Late L1
50µm
B
Lin-4p::nls::mScarlet(umn84) / +
control (no transgene)
Early L1
Embryo
o.e. MYRF-1Δ601-650 GFP (hyperactive)
20µm
20µm
C
Plin-4-GFP(maIs134)
wt
myrf-1 1-700(syb1313)
Early-Mid L1 (6h)
Late L1 (15h)
neurons
pharynx
50µm
D
Plin-4-gfp intensity
in neurons
in pharynx
Fluorescence intensity
wt
myrf-1 (syb1313)
6h
15h
E
Lin-4p::nls::mScarlet(umn84)
wt
myrf-1 1-700(syb1313)
Early-Mid L1 (6h)
Late L1 (14h)
Early-L2 (21h)
50µm
F
Lin-4p::nls::mScarlet intensity
whole body
in head neurons
in pharyngeal cells
Fluorescence intensity
Fluorescenceintensity
wt
myrf-1 (syb1313)
Early-Mid L1
Late L1
Early L2

Figure 5. Hyperactive MYRF-1 drives premature expression of *lin-4*.

A. The reporter of *lin-4* transcription, labeled by endogenously inserted *nls::mScarlet (umn84)*, which also produces a loss-of-function allele of *lin-4*. The fluorescence was not observed in embryos or early L1, but in late L1, confirming the previous reports.

B. Overexpression of a hyperactive MYRF-1 mutant, GFP::MYRF-1(delete 601-650) caused premature *lin-4* transcription in embryos and early L1, labeled by *lin-4p::nls::mScarlet*.

C. The expression of *Plin-4-GFP*(*maIs134*) in wild type and *myrf-1(syb1313)* mutants. At 6 hours, *Plin-4-GFP* expression is elevated in the neurons of *myrf-1(syb1313)* mutants but undetectable in wild type. By late L1 (15h), *Plin-4-GFP* is upregulated in multiple tissues in wild type. Although GFP expression is sustained in neurons (arrow) of the mutants, it is significantly weak or absent in the pharynx (asterisk) of the mutants.

D. The fluorescence intensity of the *lin-4* transcriptional reporter (as displayed in (C)) was measured and presented as mean ± SEM (t-test, *$p < 0.05$, **$p < 0.01$, ***$p < 0.001$). Each data point represents the mean intensity of the head neurons or pharynx region in individual animal, which were imaged using confocal microscopy.

E. The expression of *lin-4p::nls::mScarlet(umn84)* in wild type and *myrf-1(syb1313)* mutants. At 6 hours, mScarlet expression is elevated in certain neurons of *myrf-1(syb1313)* mutants but undetectable in wild type. By late L1 (14h), mScarlet is upregulated in multiple tissues in both wild type and *myrf-1(syb1313)* mutants. The mutants exhibit stronger mScarlet signals than wild type.

F. The fluorescence intensity of *lin-4p::nls::mScarlet* (as displayed in (E)) was measured and presented as mean ± SEM (t-test, *$p < 0.05$, **$p < 0.01$, ***$p < 0.001$). The ROI for "whole body" encompasses the entire body of the animal. The ROI of “in head neurons” comprises multiple head neuron nuclei in each animal. The ROI for “in pharyngeal cells” includes the 8-9 pharyngeal nuclei that exhibit strong mScarlet signals. Each data point represents the mean intensity of the ROI in individual animal.

Figure 6

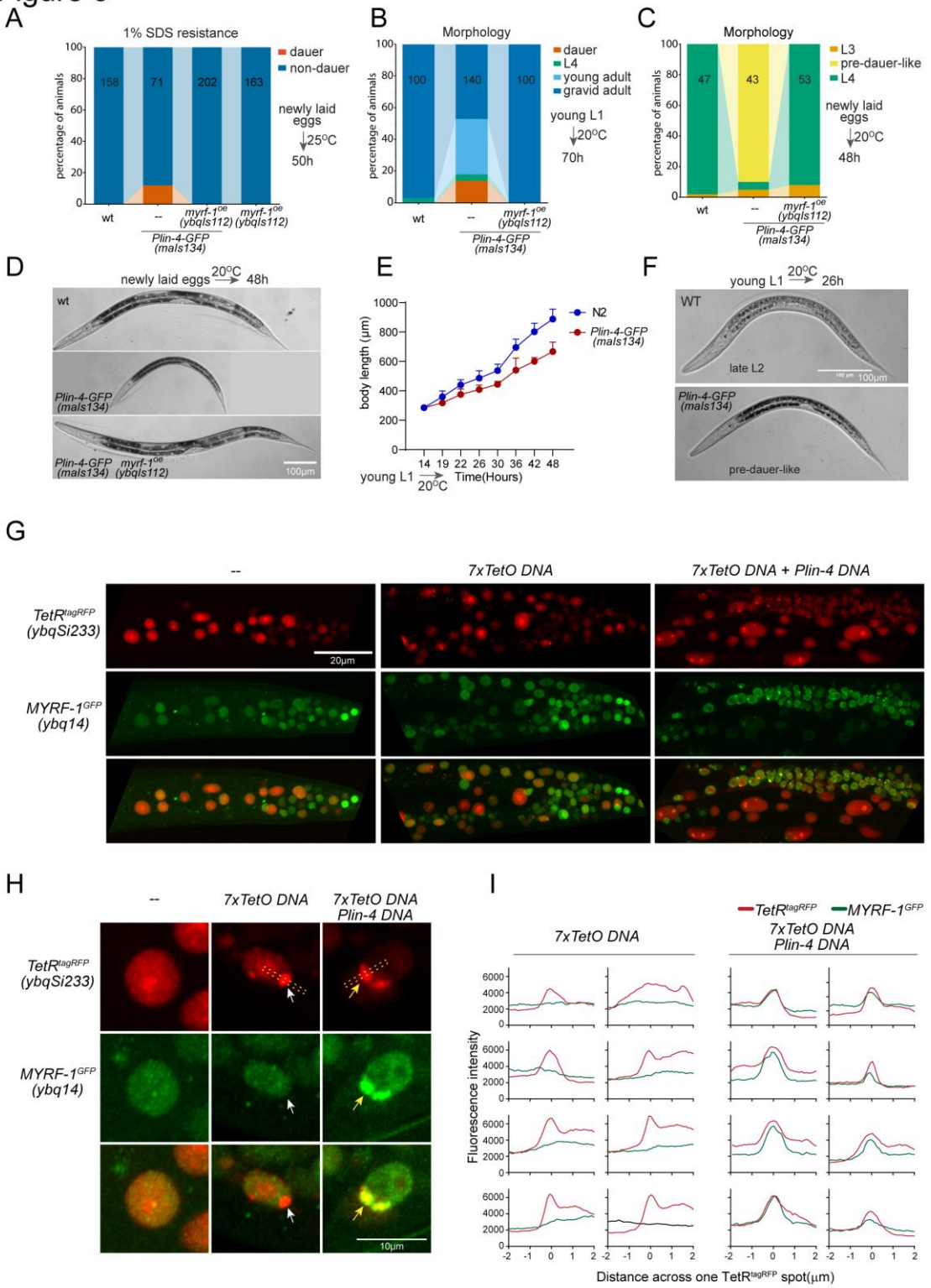
A
1% SDS resistance
percentage of animals
dauer
non-dauer
158
71
202
163
newly laid eggs
25°C
50h
wt
--
myrf-1oe (ybqls112)
Plin-4-GFP (mals134)
B
Morphology
dauer
L4
young adult
gravid adult
100
140
100
young L1
20°C
70h
C
Morphology
L3
pre-dauer-like
L4
47
43
53
newly laid eggs
20°C
48h
D
newly laid eggs 20°C 48h
wt
Plin-4-GFP (mals134)
Plin-4-GFP (mals134) myrf-1oe (ybqls112)
100µm
E
body length (µm)
N2
Plin-4-GFP (mals134)
14 19 22 26 30 36 42 48
young L1 20°C
Time(Hours)
F
young L1 20°C 26h
WT
late L2
100µm
Plin-4-GFP (mals134)
pre-dauer-like
G
--
7xTetO DNA
7xTetO DNA + Plin-4 DNA
TetRtagRFP (ybqSi233)
MYRF-1GFP (ybq14)
20µm
H
--
7xTetO DNA
7xTetO DNA Plin-4 DNA
TetRtagRFP (ybqSi233)
MYRF-1GFP (ybq14)
10µm
I
TetRtagRFP
MYRF-1GFP
7xTetO DNA
7xTetO DNA Plin-4 DNA
Fluorescence intensity
Distance across one TetRtagRFP spot(µm)

Figure 6. *lin-4* promoter DNA recruits MYRF-1 protein *in vivo*.

A. A subset of animals carrying the *maIs134* transgene constitutive dauer formation even in the absence of food depletion on culture plates. Dauer formation was assessed by treating the animals with 1% SDS for 20 minutes. MYRF-1 overexpression (*ybqIs112*) suppresses the constitutive dauer formation in *maIs134*. Animals were cultured at 20°C for 70 hours starting from freshly laid eggs. The number of animals analyzed is indicated on each bar.

B. Morphological assessment shows that a subpopulation of animals carrying the maIs134 transgene become dauer larvae, which exhibit a lean body and darkened intestine (Figure S3). MYRF-1 overexpression (*ybqIs112*) suppresses the constitutive dauer formation in *maIs134*. Animals were cultured at 20°C for 70 hours starting from young L1. The number of animals analyzed is indicated on each bar.

C. The development of *maIs134* is delayed compared to wild-type animals. with the majority of *maIs134* animals exhibiting pre-dauer-like characteristics while most of the wild-type animals become L4. While most of the wild-type animals become L4, the majority of *maIs134* animals are pre-dauer-like. Animals were cultured at 20°C for 48 hours starting from freshly laid eggs.

D. Representative images of animals from experiments in C.

E. Measurements of body length of wild type and *maIs134* animals show a growth delay in *maIs134* starting from L2. The mean body length of analyzed animals at a series of time points is shown on the graph, with the mean ± S.D. indicated. The number of animals analyzed for each data point is more than 20.

F. Representative images of animals from experiments in E. At 26h *maIs134* animals are thinner than wild type and have dark intestinal granules, which are characteristic of pre-dauer (L2d).

G. A tandem DNA array containing *lin-4* promoter (2.4 kb) DNA causes puncta of GFP::MYRF-1(*ybq14*) in the nucleus. As a control, a 7xTetO sequence-containing DNA array causes the puncta formation of TetR::tagRFP(ybqSi233), while it doesn't cause the aggregation of GFP::MYRF-1. Only the addition of *lin-4* promoter DNA causes the formation of GFP::MYRF-1 puncta.

H. Representative images of animal cells carrying transgenes described in G, but in a high magnification view.

I. Line plots of signal intensity measurements along the bar ROI drawn across one red punctum in images, examples of which were shown in H. The bar ROI is centered at the fluorescent spot and examples of bar ROI were shown in H. Each individual panel represents signals from one cell.

Figure 7

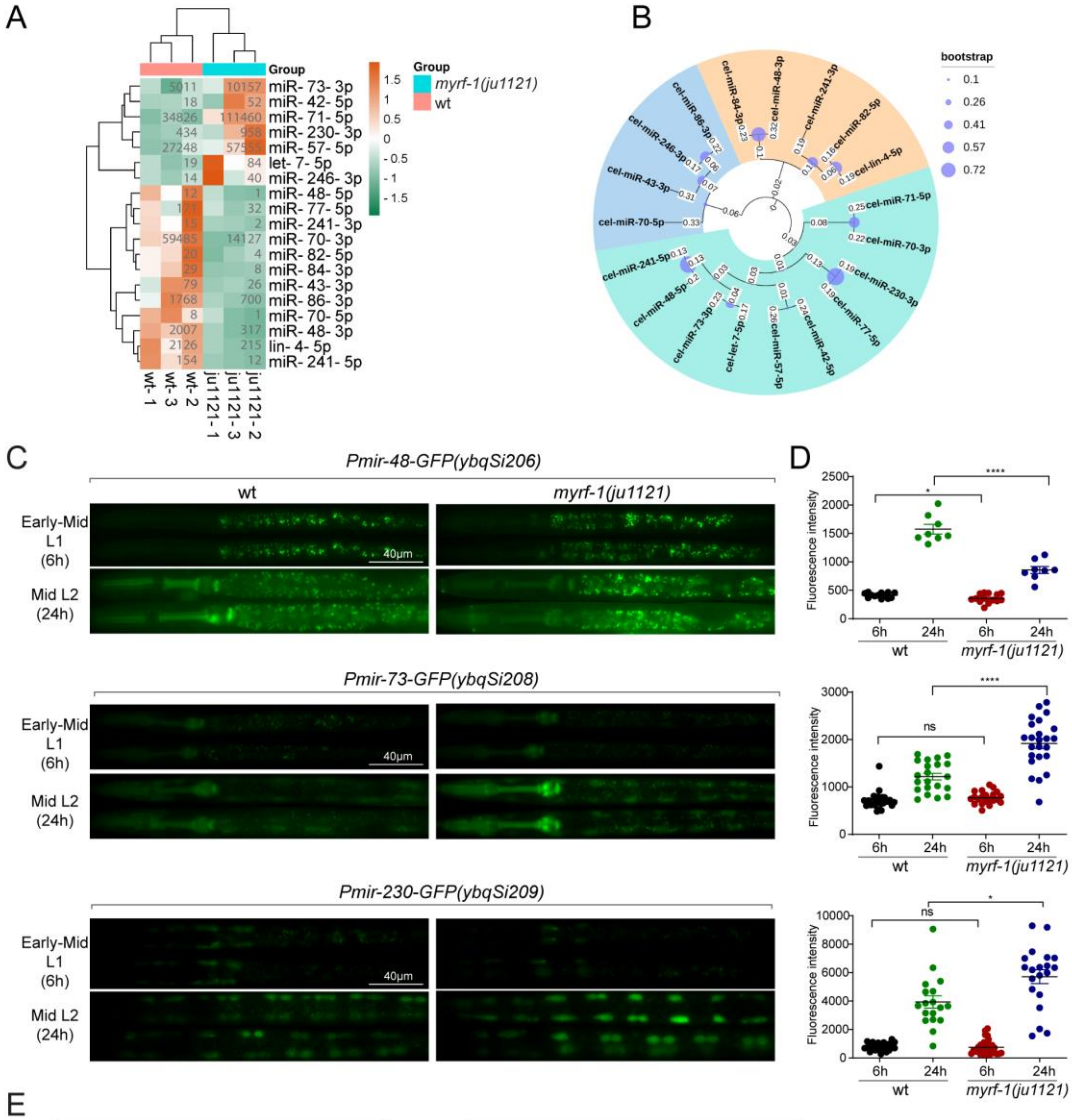
A
Group
myrf-1(ju1121)
wt
miR- 73- 3p
miR- 42- 5p
miR- 71- 5p
miR- 230- 3p
miR- 57- 5p
let- 7- 5p
miR- 246- 3p
miR- 48- 5p
miR- 77- 5p
miR- 241- 3p
miR- 70- 3p
miR- 82- 5p
miR- 84- 3p
miR- 43- 3p
miR- 86- 3p
miR- 70- 5p
miR- 48- 3p
lin- 4- 5p
miR- 241- 5p
wt- 1
wt- 3
wt- 2
ju1121- 1
ju1121- 3
ju1121- 2
B
bootstrap
0.1
0.26
0.41
0.57
0.72
cel-miR-71-5p
cel-miR-70-3p
cel-miR-230-3p
cel-miR-77-5p
cel-miR-42-5p
cel-miR-57-5p
cel-let-7-5p
cel-miR-73-3p
cel-miR-48-5p
cel-miR-241-5p
cel-miR-70-5p
cel-miR-43-3p
cel-miR-246-3p
cel-miR-86-3p
cel-miR-84-3p
cel-miR-48-3p
cel-miR-241-3p
cel-miR-82-5p
cel-lin-4-5p
C
Pmir-48-GFP(ybqSi206)
wt
myrf-1(ju1121)
Early-Mid L1 (6h)
Mid L2 (24h)
40μm
Pmir-73-GFP(ybqSi208)
Pmir-230-GFP(ybqSi209)
D
Fluorescence intensity
6h
24h
wt
myrf-1(ju1121)
ns
E
Early L1
PAN-1
MYRF
ICE
DNA binding
Nucleus
lin-4
Late L1
?
N-MYRF
miRNA lin-4

Figure 7. MYRF-1 regulates a selective subset of microRNAs during L1-L2 transition.

A. The hierarchical clustering diagram shows differential miRNA expression levels in wild-type and *myrf-1(ju1121)* animals at L2 stage. The color scale represents the log2 of the fold change, with red indicating highly expressed miRNAs and blue indicating low-expressed miRNAs. The numbers indicate the mean TPM of the specific miRNA from three replicates. Significance was determined at $P<0.05$.

B. The phylogenetic analysis shows the relationship between differentially expressed miRNA genes in *myrf-1(ju1121)*. The three branches are color-coded.

C. The expression of transcriptional reporters, *Pmir-48-gfp(ybqSi206)*, *Pmir-73-gfp(ybqSi208)*, and *Pmir-230-gfp(ybqSi209)* in wild-type and *myrf-1(ju1121)* animals at early-mid L1 (6h) and middle L2 (24h) is shown.

D. The fluorescence intensity of transcriptional reporters shown in (C) is quantified and presented as mean ± SEM (t-test: ns, not significant, *$p<0.05$, ****$p<0.0001$); $n >10$, where n is the number of animals analyzed.

E. An illustration for how MYRF is processed and promotes *lin-4* expression during development. At early L1, MYRF is mainly localized to the cell membrane in a PAN-1 dependent manner. However, during late L1, N-MYRF is released from the membrane through the catalytic activity of the ICE (Intramolecular Chaperone of Endosialidase) domain following its trimerization. Subsequently, N-MYRF translocates to the nucleus to enhance the transcription of *lin-4*.

Figure S1

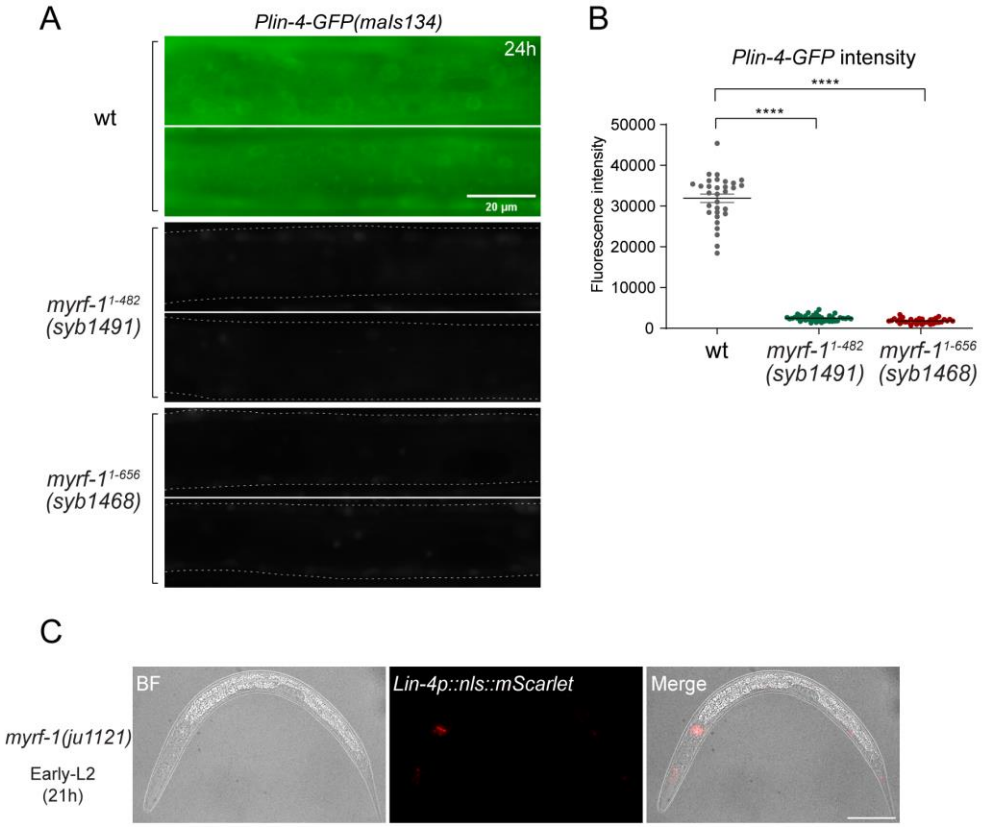
A
Plin-4-GFP(maIs134)
24h
wt
20 µm
myrf-1 1-482 (syb1491)
myrf-1 1-656 (syb1468)
B
Plin-4-GFP intensity
****
****
Fluorescence intensity
50000
40000
30000
20000
10000
0
wt
myrf-1 1-482 (syb1491)
myrf-1 1-656 (syb1468)
C
myrf-1(ju1121)
Early-L2 (21h)
BF
Lin-4p::nls::mScarlet
Merge

Figure S1. *Plin-4-GFP* expression in *myrf-1* loss of function mutants.

A. *Plin-4-GFP*(*maIs134*) expression was examined in wild-type, *myrf-1*(*syb1491*), and *myrf-1*(*syb1468*) animals at the L2 stage (24h). *Plin-4-GFP* was not detected in *myrf-1* mutants.

B. The fluorescence intensity of *Plin-4-GFP* was quantified and presented as mean ± SEM (t-test; ****$p<0.0001$); $n > 30$, where n is the number of animals analyzed.

C. An individual of *myrf-1(ju1121)* mutant, showing DIC image and *lin-4p::nls::mScarlet(umn84)* fluorescence. mScarlet is expressed in 8-9 pharyngeal nuclei.

Figure S2

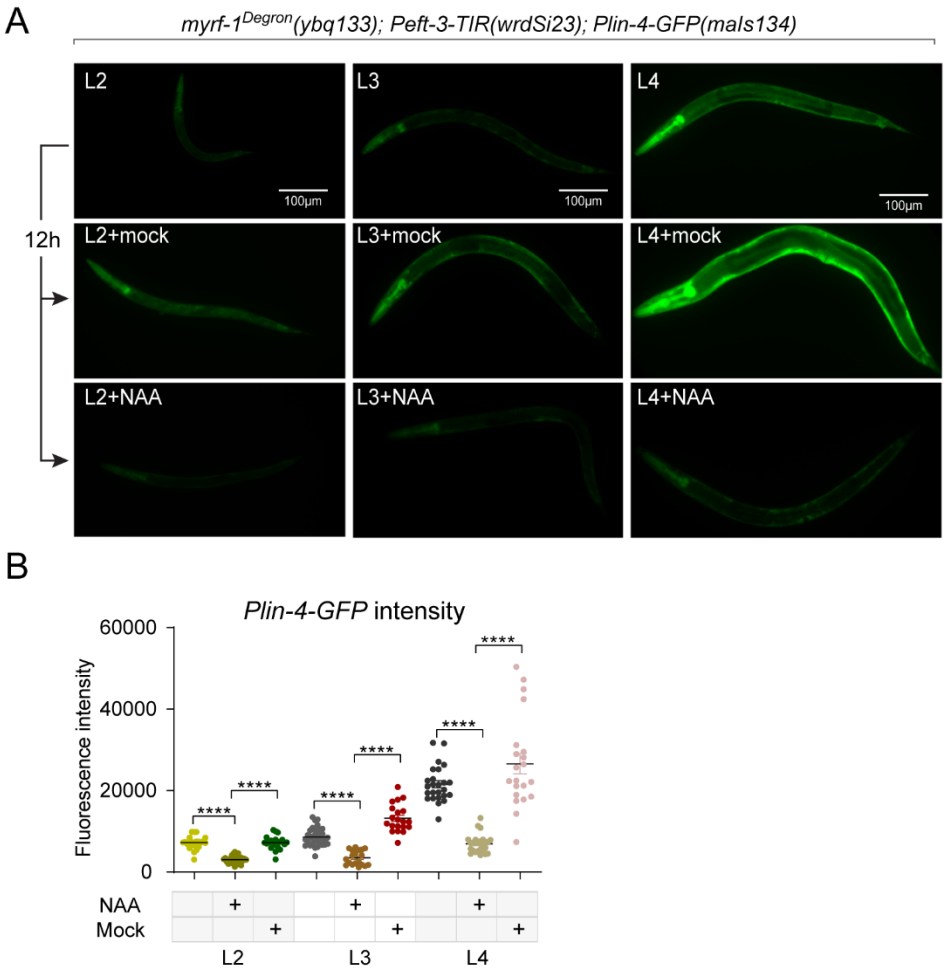

Figure S2. MYRF-1 is required for *lin-4* transcription in all larval stages.

A. Larval stages L2, L3, and L4 animals were treated with or without 4 mM K-NAA for 12 h. The *lin-4* transcription reporter was down-regulated in the drug-treated animals compared to the pre-treated and mock-treated animals.

B. The fluorescence intensity of *lin-4* transcription reporter was quantified and presented as mean ± SEM (t-test; ****p<0.0001); n >30, where n is the number of animals analyzed.

Figure S3

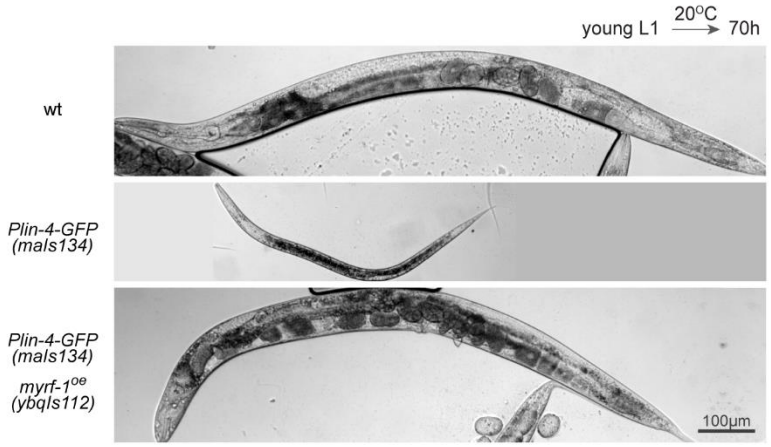

Figure S3. Constitutive dauer phenotype observed in a subpopulation of *Plin-4-GFP*(*mals134*) animals.

Representative images of animals from the experiments in Figure 4B, which were cultured at 20°C for 70 hours, starting from synchronized young L1 larvae. A subset of animals carrying the *mals134* transgene exhibited a constitutive dauer phenotype even when food was not depleted on the culture plate.

Figure S4

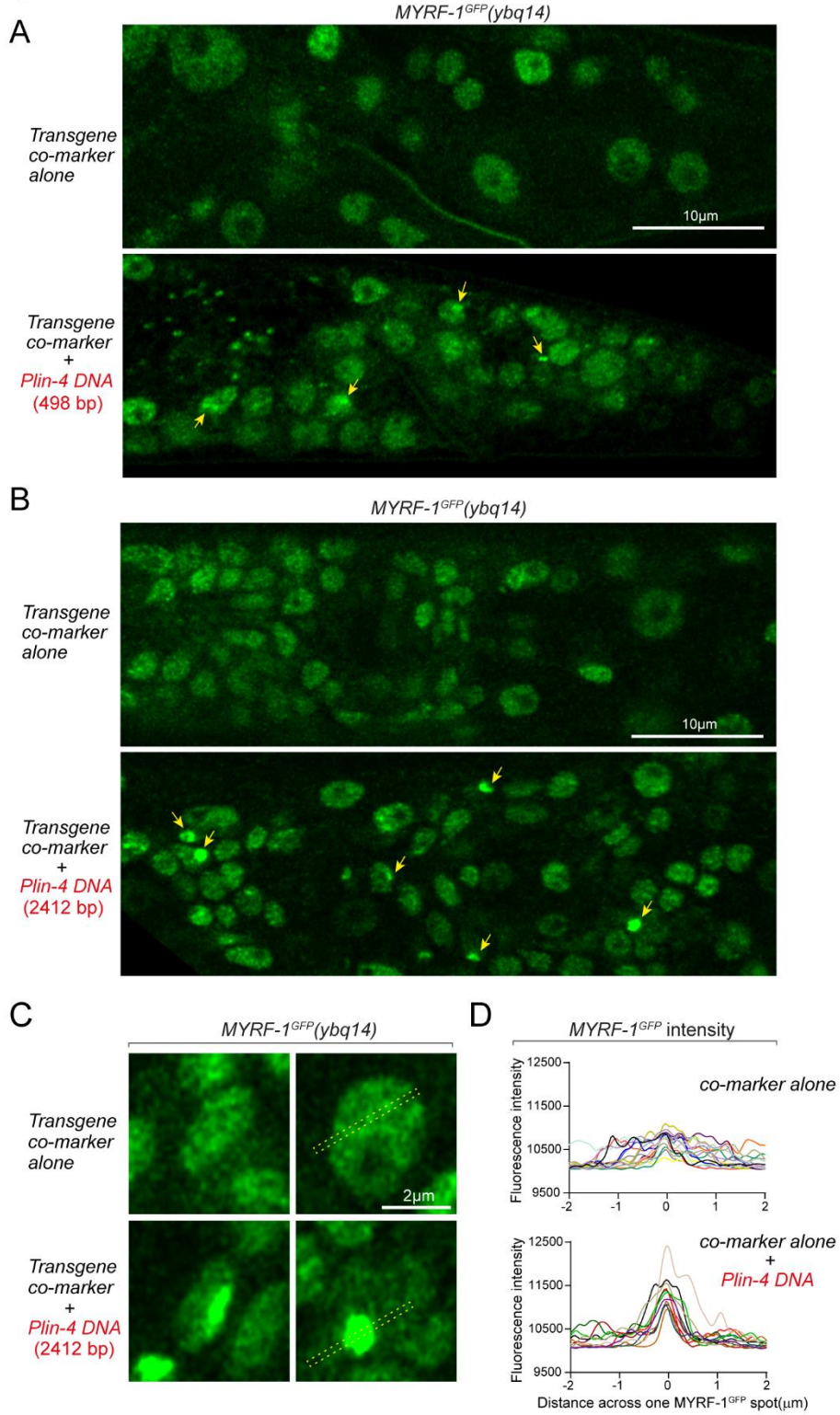
A
MYRF-1GFP(ybq14)
Transgene co-marker alone
10μm
Transgene co-marker + Plin-4 DNA (498 bp)
B
MYRF-1GFP(ybq14)
Transgene co-marker alone
10μm
Transgene co-marker + Plin-4 DNA (2412 bp)
C
MYRF-1GFP(ybq14)
Transgene co-marker alone
2μm
Transgene co-marker + Plin-4 DNA (2412 bp)
D
MYRF-1GFP intensity
co-marker alone
Fluorescence intensity
12500
11500
10500
9500
-2
-1
0
1
2
co-marker alone + Plin-4 DNA
Distance across one MYRF-1GFP spot(μm)

Figure S4. *lin-4* promoter DNA causes aggregation of GFP::MYRF-1(*ybq14*) in the nucleus.

A. Tandem DNA arrays containing *lin-4* promoter (498 bp) DNA caused aggregation of GFP::MYRF-1(*ybq14*) in the nucleus (arrow), while a control co-marker (*Pmyo-2-mCherry*) containing DNA array did not cause the aggregation of GFP::MYRF-1.

B. Tandem DNA arrays containing *lin-4* promoter (2.4 kb) DNA caused aggregation of GFP::MYRF-1(*ybq14*) in the nucleus (arrow), while a control co-marker (*Pmyo-2-mCherry*) containing DNA array did not cause the aggregation of GFP::MYRF-1.

C. Representative images of animal cells carrying transgenes described in B, but in a high magnification view.

D. Line plots of signal intensity measurement along the bar ROI drawn across the GFP spots as illustrated in representative images in C. The bar ROI is centered at one fluorescent punctum. Each individual line represents signals from one representative cell. Examples of bar ROI were drawn on the images in C.